Aging and Disease
www.aginganddisease.org
Early access date: August 10, 2026
http://dx.doi.org/10.14336/AD.2026.0357

Original Article

# Single-Nucleus RNA-Seq of Human and Rat Cardiomyocytes Identifies Shared and Distinct Regulators and Features of Aging and Disease

**Samaneh Ekhteraei-Tousi[1#,&], Rosa Doñate Puertas[1#,&], Mohamad Youness[1], Onne A.H.O. Ronda[1], Magnus Aronsen[2], Emil K. S. Espe[2], Arne Olav Melleby[2], Ida Marie Hauge-Iversen[2], Ella Cutsforth[1], Lirong Li[1], Emma L. Robinson[1&], Einar Sjaastad Nordén[2], Mani Sadredini[2&], Filip Rega[3,4], Kenneth C. Bedi Jr[5], Kenneth B. Margulies[5], Karin R. Sipido[1], Ivar Sjaastad[2], H. Llewelyn Roderick[1,6*]**

[1]Laboratory of Experimental Cardiology, Department of Cardiovascular Sciences, KU Leuven, Leuven 3000, Belgium. [2]Institute for Experimental Medical Research, Oslo University Hospital and University of Oslo, Oslo, Norway. [3]Laboratory of Cardiac Surgery, Department of Cardiovascular Sciences, KU Leuven, Leuven, Belgium. [4]Department of Cardiac Surgery, University Hospitals Leuven, Herestraat 49, 3000 Leuven, Belgium. Leuven, Belgium. [5]Cardiovascular Institute, Perelman School of Medicine, University of Pennsylvania, Philadelphia, PA, USA. [6]Leuven Institute for Single Cell Omics (LISCO), KU Leuven, Leuven 3000, Belgium.

[Received March 27, 2026; Revised August 2, 2026; Accepted August 4, 2026]

**ABSTRACT: Age is the greatest risk factor for cardiovascular diseases, including heart failure (HF), which is a leading cause of morbidity and mortality. While left ventricular fibrosis, hypertrophy and decreased contractility are associated with cardiac aging, age is not sufficient for HF development. Despite diminished cardiomyocyte (CM) function being central to cardiac pathology, whether factors predisposing the aged CM to disease are the same or distinct from those underlying disease are not determined. To address this, we integrated our own and published single-nucleus RNA-Seq data of different cardiomyopathies and from young and old human samples and probed for unique and overlapping features. To test the utility of rodents for modelling human aging and disease, we compared human data with data from deeply phenotyped relevant rat models. We identified diverse CM substates, which were significantly altered in proportion with pathology in human and in both pathology and age in rat. In human and rat, CM exhibited substantial transcriptomic changes with age and pathology. In addition to established hallmarks of cardiomyopathy and aging, we detected etiology/age-specific differentially expressed genes/pathways and identified candidate nodal regulators underlying these changes. In human and rat, CM exhibited greater cellular and transcriptional heterogeneity in pathology and age. While rats showed substantial differences to humans, overlapping features, including increased CM heterogeneity and altered expression of genes related to epigenetic, fibrotic and hypertrophic remodelling, were also detected. Although some pathways, differentially expressed genes and trajectories are shared between age and pathology, unique aspects support age and pathology as distinct entities.**

***Keywords:*** Heart failure, cardiac aging, cardiomyocyte remodelling, single-cell/single-nucleus RNA-Seq, cellular heterogeneity, meta-analysis

***Correspondence should be addressed to:** Prof. H. Llewelyn Roderick, Department of Cardiovascular Sciences, KU Leuven, Leuven 3000, Belgium. Email: llewelyn.roderick@kuleuven.be. [#]These authors contributed equally. [&]Current address: SE-T: Department of Immunology and Infection, Biomedical Research Institute, Hasselt University, Hasselt, Belgium. RDP, Université Paris Cité et Université Sorbonne Paris Nord, INSERM U1148, LVTS, Paris, France. ELR, Edwards Lifesciences, Irvine, California, USA. MS: Faculty of Health Sciences, Department of Nursing and Health Promotion, Oslo Metropolitan University, Oslo, Norway

## INTRODUCTION

Cardiovascular diseases (CVD) including heart failure (HF), remain the leading cause of mortality and morbidity worldwide. The greatest risk factor for CVD is age, with CVD risk doubling for every decade of life after 60 [1, 2]. With a doubling of the global population over 60 by 2050, without significant improvements in treatment, the number of CVD-related deaths will significantly rise. Factors contributing to the increased susceptibility and reduced resilience of the aging heart in the face of pathological cues remain incompletely understood. However, better understanding of the basis of resilience of unaffected individuals provides insight into disease mitigation.

Notably, aging is accompanied by remodeling of the heart associated with alterations in muscle mass and increased fibrosis that together can lead to decreased cardiac function, greater myocardial stiffness and an increased risk of arrhythmia [3, 4]. At the cellular level, this involves a net loss of cardiomyocytes (CM), owing to their lack of proliferative capacity, hypertrophy of remaining CM to compensate, and increased deposition of extracellular matrix (ECM) by fibroblasts (FB) [3]. Changes in CM physiology and metabolism similar to those observed in pathology also occur with aging [3-5]. However, owing to the ability of the heart to compensate and tolerate these age-related changes [6], deleterious consequences are not necessarily observed, and cardiac function is preserved. Nevertheless, these alterations may reduce cardiac resilience, increasing its vulnerability to additional stressors that in turn contribute to functional decline and eventual HF.

To understand the molecular basis of this tissue remodelling, gene expression studies have been performed and uncovered alterations in key pathways, including those involved in growth factor signaling, mitochondrial pathways, DNA damage, and senescence [7, 8]. However, the use of bulk tissue RNA in many of these analyses precludes identification of cell-type specific changes, limiting mechanistic insight. For example, bulk analysis does not permit detection of alterations in the relative proportions of the different cardiac cell types, which could, in the absence of transcriptomic changes in each cell type, affect the tissue transcriptome [9]. Moreover, excluding cell-type specific genes, bulk transcriptomic approaches do not reveal cell-type–specific information, precluding the uncovering of phenotypic or transcriptomic remodeling within individual cardiac cell types and their contributions to changes in cardiac function [10, 11]. Further, neither tissue-based or cell-type specific analysis capture the transcriptional heterogeneity that may underline phenotypic variability among individual cell types or differences in specific transcripts that may give rise to new cell states or that contribute to disease processes [9, 12] .

Deleterious remodeling and death of CM are central to the diminished contractile function and greater arrhythmia propensity of the diseased heart [13]. In advanced age, while not as severe as in pathology, a decline in cardiac function with features overlapping with pathological hypertrophy, including impaired relaxation and diminished β-adrenergic responsiveness, is detected [14]. Moreover, rodent studies indicate that the underlying hypertrophy of aged CM compromises their additional responsiveness to pathological cues [15]. Recent single-cell and single-nucleus (sn) RNA-Seq analysis has revealed CM subpopulations/states that vary in proportion between health and disease [16], as well as distinct CM gene programs underlying remodeling in cardiac hypertrophy and failure [17-20]. In animal models of disease, snRNA-Seq has enabled detection of increased CM heterogeneity, which has been invoked as a contributor to greater arrhythmia propensity [21]. While low-throughput analysis of individual genes has revealed increased transcriptional heterogeneity in aged rodent CM [12], how the proportion of different CM states and heterogeneities of cell types and gene expression change with human aging are not determined. It remains unclear whether aging- and pathology-associated CM remodeling represent distinct entities or represent early and later stages along a shared trajectory toward HF.

Here we set out to identify transcriptional features of CM during aging and determine whether they overlap or are distinct from those across different cardiomyopathies (CMPs). Through these analyses, we aimed to gain insights into aspects of remodeling that predispose the aged heart to future disease, i.e. decrease its robustness. Using in-house generated snRNA-Seq data [22] supplemented with published datasets from human hearts [17-20], we compared the transcriptomic changes in CM from aging hearts with no reported cardiac pathology with those associated with acquired and genetic CMPs (ischemic cardiomyopathy (ICM), dilated cardiomyopathy (DCM), and hypertrophic cardiomyopathy (HCM)). To test the utility of rodents for such studies, often used to mitigate against comorbidities in human, we analyzed transcriptomic changes in CM from aged rats and from rats subjected to pressure overload. We identified distinct CM populations in human and in rat that were differentially affected by disease and age. In both species, CM heterogeneity was increased with age and disease, which was also associated with greater transcriptional variance in human. Aging and disease involved extensive transcriptional remodeling related to alterations in key cellular pathways and processes notably in calcium handling, metabolism and in

epigenetic regulation. While aging was clearly distinct from human CMP, it most closely resembled remodeling associated with HCM, and showed overlap with rats subjected to a mild pressure overload insufficient to induce HF. Together, our analysis thus identifies candidate targets that discriminate and that are shared between cardiac aging and disease and highlights the value of animal models to study human aging.

## MATERIALS AND METHODS

**See also Extended Methods in the Supplementary file**

### Human Heart Tissue Collection and Ethics

Human heart samples used for 10x Genomics analysis were from the UZ/KU Leuven Biobank cardiac tissue collection that is generated through a collaboration between the Laboratory of Experimental Cardiology, the UZ transplant team and the Cardiac Surgery Department of UZ Leuven. The study protocol conformed to the Helsinki declaration and was conducted according to national and European Union regulations on the use of human tissues. This study was approved by the ethics committee of UZ Leuven (S58824). The majority of the HF hearts used in this study were from patients undergoing cardiac transplantation at UZ Leuven. Non-failing (NF) cardiac tissue samples were from organ donors whose hearts were not allocated for transplant for reasons of age, medical or technical reasons, and/or from hearts from which only valves were harvested. Hearts were designated as NF, including aged samples, owing to absence of pathology recorded in associated medical files and normal organ appearance at time of harvesting. NF hearts were collected as part of a multi-organ retrieval during which cold preservation solution was infused through the aorta for preservation of abdominal and/or thoracic organs. Cardiectomy is performed while systemic cold preservation perfusion is ongoing after which hearts are immediately placed in sterile cardioplegic solution (130 mM NaCl, 6 mM HEPES, 1.2 mM $MgSO_4$, 27 mM KCl, 10 mM glucose, pH 7.2 in ultrapure water). Tissue samples were taken from the LV anterior and posterior wall, avoiding scar tissue. Mid-myocardium, without epi- and endocardium, was snap-frozen in liquid nitrogen and stored at −80°C for later analysis. Additional transmural LV free wall myocardial samples included in the RT-qPCR analysis were procured from the Human Heart Tissue Biorepository at the University of Pennsylvania. Samples were procured using previously described consent and cardioprotection routines [23, 24]. Briefly, all samples were collected in accordance with protocols and ethical regulations approved by Institutional Review Boards at the University of Pennsylvania and the Gift-of-Life Donor Program (PA, USA). All donors received in situ antegrade cold cardioplegia and were stored on wet ice in cold saline until flash frozen in liquid nitrogen. For the gene expression analysis by RT-qPCR, tissues were from NF young (Y; 20-44 years, n=37, 19 female), and non-failing old (O; 65-94 years, n=88, 38 female), ICM (n=41, 5 female), HCM (n=22, 9 female), and DCM (n=62, 21 female). NF middle-aged (45-64 years) served as an age-matched control group for the cardiomyopathies (n=41, 19 female) (Table 1, Supplementary File 1). Samples on which 10x snRNA-Seq was performed are as recently described [GSE298023] [22], and include 4 NF, 5 ICM and 4 DCM samples.

### Aging rats

Male Sprague Dawley (SD) rats (Harlan Sprague Dawley Inc. (now Envigo), USA) were housed in a temperature-controlled room with a 12 h/12 h light/dark cycle according to the animal experimental protocol approved by the Norwegian Animal Research Authority (FDU applications 4318 and 20208). At 3 or 26 months, cardiac function and geometry were assessed by echocardiography and magnetic resonance imaging (MRI). Hearts were excised and weighed at time of euthanasia. LVs were immediately snap-frozen in liquid nitrogen before storage at -80 °C. LV samples were also fixed in 10% formaldehyde and then embedded in paraffin for histological studies.

### Pressure overload by banding of the ascending aorta in rats

6-week-old male SD rats were subjected to constriction (banding) of the ascending aorta (AB) for 6 weeks. The animal experimental protocol used in this study was approved by the Norwegian Animal Research Authority (FDU applications 4318 and 20208) and has been previously described [25]. Mild and severe stenosis was induced using spliced nitrile rubber O-rings of fixed internal diameter 1.5 mm (loose) or 1.07 mm (tight) respectively, which were placed around the ascending aorta proximal to the brachiocephalic trunk. Sham-operated animals (S) served as controls and underwent the same surgical procedure, excluding the placement of the O-ring. Immediately prior to euthanasia, cardiac function and geometry were assessed by echocardiography and MRI. At euthanasia, hearts were excised and weighed. The LV tissue was divided, where one part was snap-frozen in liquid nitrogen and immediately stored at -80 °C, and the other part was fixed in 10% formaldehyde and then embedded in paraffin for histological studies.

**Histological assessment of fibrosis in rat cardiac tissue**

Paraffin sections (6 µm) were cut using a microtome (Epredia HM 355S, Thermo Fisher Scientific Inc., Waltman, MA, USA). The sections were stained using Masson's trichrome (BenchMark Special Stains, Ventana Medical Systems, Inc., Tucson, AZ, USA). High-resolution images were acquired using an automated slide scanner system. Fibrosis was quantified with QuPath-0.4.3 [26]. Correct masking and fibrosis detection were confirmed by visual inspection. All image analysis was performed by a single operator blinded to animal group.

**Isolation of cardiac cell nuclei used in RT-qPCR and VASA-Seq experiments**

Debris-free suspensions of intact cardiac cell nuclei were generated by tissue homogenization followed by sucrose gradient centrifugation, and flow sorting with all steps performed at ≤ 4 °C, as we have previously described [11] and with modifications from Preissl et al. [10]. Nuclei were sorted using a BD Influx flow cytometer either into tubes for qPCR or into 384-well hardshell plates (BioRad), when snRNA-Seq (VASA-seq) was applied. Intact debris-free CM nuclei were harvested by setting gates for DAPI+ve, PCM1+ve, and PLN+ve. For collection in tubes, CM nuclei were sorted into PBS containing 400 µg/mL UltraPure™ BSA (Thermofisher Scientific, AM2616). Sorted CM nuclei were flash-frozen with 700 µL Qiazol. For collection into 384-well plates, before cell sorting, each well was pre-filled with 5 µL of mineral oil (Sigma-Aldrich) and 50 nL of CEL-seq2/VASA-seq [27, 28] primers at a concentration of 0.25 µM. After sorting, plates were sealed and centrifuged at 1,500 x g for 2 min before storage at −80 °C.

**mRNA isolation and reverse transcription quantitative PCR (RT-qPCR)**

Total RNA for RT-qPCR experiments was extracted from the nuclei of CMs and mid-myocardial LV tissue of aging and AB rats using Qiazol/TRIzol, as well as from mid-myocardial LV tissue of humans, but using Qiazol. RNA extracted from the nuclei of aged and AB rat CMs was treated with DNase using the TURBO DNA-free™ kit (Thermo Fisher Scientific) and subsequently reverse-transcribed into cDNA using SuperScript™ IV Reverse Transcriptase (Thermo Fisher Scientific). PrimePCR assays were validated by Bio-rad. RT-qPCR was performed using Sso Advanced Universal Sybr Green supermix. For LV tissue samples, total RNA was isolated and 1 µg reverse-transcribed using SuperScript™ III Reverse Transcriptase (Thermo Fisher Scientific). qPCR was performed using GoTaq® qPCR Master Mix (Promega). Primer sequences used in these experiments are detailed in Table 2. Relative quantities were calculated using the ΔΔCT method, normalized to the appropriate reference genes, and expressed as -ΔΔCT values. qPCR reactions were performed using a CFX384 Touch™ Real-Time PCR Detection System (Bio-Rad, Temse, Belgium). For rats, gene expression data were normalized to reference genes 18S, GAPDH, RPL32, SDHA, TBP. The stability of reference genes was established using geNORM [29].

**snRNA-Seq - VASA-seq, Vast Transcriptome Analysis of Single Cells by dA-Tailing**

High-throughput total RNA sequencing in single nuclei using VASA-seq was performed according to Salmen et al. [30] by Single Cell Discoveries (Utrecht, the Netherlands) for the rat single CM nuclei RNA-seq. The barcoded pooled libraries were sequenced by Illumina Nextseq 500.

**snRNA-Seq - 10x Genomics**

Human cardiac nuclei were isolated and 10x RNA-Seq libraries were prepared as outlined by Amoni et al. [21, 22, 31]. Libraries were prepared on ~6,000 nuclei per sample (10x Genomics) and sequenced at a targeted depth of 80,000 reads per nucleus.10x RNA-Seq data from these samples focusing on FB were recently described [GSE298023] [22].

**snRNA-Seq data processing**

Detailed bioinformatic methods for processing, aligning and integration of the 10x snRNA-seq and VASA-seq datasets are provided in the Supplementary Methods. For human, four previously published snRNA-Seq datasets (summarized in Table 3) [3, 23-26], and our own described above, were aligned to the GRCh38 reference genome and merged. Rat datasets were aligned to the Rnor_6.0 reference genome.

Cell-type proportions in human were calculated per donor and summarized as mean donor-level proportions. CM nuclei were annotated by transferring labels from the Human Cell Atlas [20] reference using Seurat transfer anchors and assigned to the ventricular CM state with the highest prediction score. Because CM states represent a transcriptional continuum, no prediction score threshold was applied. Statistical comparisons of human cell-type and CM subpopulation proportions were performed at the donor level using two-sided Wilcoxon rank-sum tests with Benjamini-Hochberg false discovery rate (FDR) correction.

Following quality control, CM nuclei from the left ventricles of rat hearts (three biological replicates per group) were batch-corrected and integrated using Harmony. CM nuclei were subsequently clustered using Seurat's graph-based clustering algorithm (FindClusters, algorithm = 3), and CM subpopulations were annotated based on canonical marker gene expression.

**Analysis of cell and transcriptional heterogeneity.**

CM heterogeneity was assessed by calculating Euclidean distances in principal component (PC) space derived from the integrated single-nucleus RNA-sequencing dataset. For aging analyses, heterogeneity was quantified and statistically compared at the nucleus level. For age-matched disease comparisons, heterogeneity was summarized at the donor level to account for biological replication. Statistical significance was assessed using two-sided Wilcoxon rank-sum tests with Benjamini-Hochberg false discovery rate (FDR) correction.

Transcriptional variability was evaluated using the 2,000 highly variable genes (HVGs) identified in the merged dataset. Gene-wise standardized variance (vst. variance.standardized) was recalculated independently for each comparison group using Seurat's variance-stabilizing transformation (VST). For the comparison between Y and O samples, variance distributions were calculated from all nuclei within each age group. For comparisons between NF and CMP samples, variance was recalculated independently for each donor and subsequently pooled within each condition to account for inter-sample variability. Statistical comparisons were performed using two-sided Wilcoxon rank-sum tests. Due to the lower number of cells and biological replicates, rat analyses were performed at the nucleus level.

**Trajectory analysis**

The transcriptome profile shifts across the age groups and pathologies were analysed with the Slingshot (v 2.2.1) package in R [32]. This process involves two main steps: first, identifying the global lineage structure using a cluster-based minimum spanning tree, and second, fitting simultaneous principal curves to describe each lineage.

**Pseudo-bulk analysis of RNA-Seq data**

To identify DEGs across conditions, gene counts from all nuclei per sample were summed to generate pseudo-bulk RNA-seq data. This process mitigates against false positive discoveries, or type 1 errors, arising from the sparsity and heterogeneity inherent in single-cell data [33, 34].

**Principal Component Analysis (PCA)**

Following the preprocessing and batch effect removal, the corrected gene count values were subjected to PCA by 'factoextra' package (v1.0.7) [35] to identify major sources of variation and ensure the absence of any remaining batch effects or outliers.

**Batch effect removal and differential gene expression (DEG) analysis**

To minimize the impact of potential technical batch effects in pseudo-bulk data analysis, the "combat" function from "sva" (surrogate variable analysis) package (v 3.42) [36] was employed to harmonize the gene expression profiles between the samples in each experiment set across different batches while preserving the biological differences. The robust DEGs between the specific experimental conditions were identified using edgeR (v 3.36), through glmQLF [37-39]. The age-matched groups included as a covariate in the design matrix of the comparisons of the CMPs and NF heart CMs, allowing us to account for age effects across all comparison groups. We then identified consistently differentially expressed genes (DEGs) by selecting those that were reproducibly significant across the different age groups. The genes with a false discovery rate (FDR) < 0.05 and log2 fold change (logFC) > 0.25 and < - 0.25 were detected as DEGs.

**Functional enrichment analyses**

The enriched functional categories (padj < 0.05) associated with the identified DEGs were determined using the "enrichGO()" function from the clusterProfiler v 4.2.0 [40, 41] and enrichR v3.0 [42].

**Motif enrichment analyses**

RcisTarget (v1.14.0) [43, 44] was used to identify the enriched transcription factor (TFs) binding motifs and their target genes on the list of DEGs per each comparison. The significant motifs for special TFs with a normalized enrichment score (NES) threshold higher than 2.5 were identified for the genes.

**Overlap analysis**

The shared and exclusive genes between the comparisons were detected and visualized through Venn v1.10 [45] and GOplot v 1.0.2 [46]. UpSetR v1.4.0 package was used to visualise the intersections between more than three categorical vectors [47].

**Correlation analysis**

The correlation between conditions was assessed using Spearman's Rank-Order correlation of the detected DEGs in each comparison, performed with PerformanceAnalytics v 2.0.4 [48].

**Weighted gene correlation network analysis (WGCNA)**

To detect potential co-regulated genes that show distinct patterns across the conditions, we applied a weighted correlation analysis using WGCNA v1.70-3 [49], and identified their function by enrichment analysis (enrichR). WGCNA was performed on DEG-defined gene sets rather than the full expression matrix since the goal was identification of co-expression structure within genes already associated with aging, CMP, or their overlap. This approach reduces the contribution of genes with low variance or limited relevance to the comparisons of interest and facilitates interpretation of modules in relation to the DEG and pathway analyses. However, because preselecting DEGs can influence module composition and connectivity, WGCNA-derived modules and hub genes were interpreted as candidate co-expression features within DEG-defined programs rather than as global regulatory networks. The spatial positions of the nodes (genes) and edges (interactions) were computed using igraph v1.4.2 [50] and then visualized using ggraph v2.0.5 [51].

**GWAS, eQTL, and transcriptome data integration**

To identify DEGs associated with CVD in the aging process, we integrated GWAS, eQTL (expression quantitative trait locus), and our transcriptome data. For this, GWAS associations were downloaded from the NHGRI-EBI GWAS Catalog for the "cardiovascular disease" trait EFO_0000319 including child traits (www.ebi.ac.uk/gwas/efotraits/EFO_0000319). Multi-SNP entries were expanded to one rsID per row and we parsed p-values, effect sizes (OR/BETA), risk-allele frequency, the "strongest SNP–risk allele," and 95% CIs. Cardiac eQTL summary statistics were also obtained from GTEx v8 for Heart-Left Ventricle (https://ftp.ebi.ac.uk/pub/databases/spot/eQTL/imported/GTEx_V8/ge/Heart_Left_Ventricle.tsv.gz). GWAS and eQTL were merged by rsID and harmonized by comparing the GWAS effect/risk allele to the eQTL ALT/REF; eQTL betas were sign-flipped when the GWAS effect matched the REF, and ambiguous A/T or C/G sites were removed only if harmonization was unresolved. Significant genetic instruments (SNPs) were defined as variants meeting genome wide significance in GWAS ($p < 5\times10^{-8}$) and nominal significance as eQTL ($p < 1\times10^{-5}$), retaining the most significant eQTL per (rsID, gene). Ensembl gene IDs were mapped to HGNC symbols via Ensembl BioMart (version suffixes removed). GWAS traits were heuristically grouped into ICM, HCM, and DCM using keyword matching, excluding congenital terms. Contrasts between snRNA-seq DEG for aging, ICM, HCM, and DCM provided logFC and direction. We defined directional concordance as risk↑expr (positive harmonized eQTL beta) with DEG up, or risk↓expr with DEG down; true concordance additionally required GWAS trait-class = condition for ICM/HCM/DCM, while aging used the directional rule only. Per gene and condition, we retained the best eQTL p-value. Finally, UpSet plot contrasting disease-class GWAS gene sets with true-concordant snRNA sets was visualized.

**Identification of orthologous genes between human and rat**

To integrate the human and rat datasets, orthologous genes between species were identified through biomaRt v2.50.1 [52] and getLDS function.

**Data visualization**

Graphs were either prepared with tidyverse v1.3.1 [53] and dplyr v 1.0.7 [54] and visualized with ggplot2 v3.4.0 [55] or built-in functions in R or were generated in PRISM version 11.

**Statistical analysis**

For normally distributed data, two-sided, unpaired Student's t-tests were applied for two-group comparisons, while Wilcoxon rank-sum tests were used for non-normally distributed data. Analyses involving more than two groups employed one-way ANOVA with a post hoc Tukey test for Gaussian-distributed data, and the Kruskal-Wallis test with a post hoc Dunn's test for non-Gaussian-distributed data. Significance levels were visualized using the ggpubr package v0.4.0 [56] or using Prism v9.4.0 on the graphs for each comparison. Data were deemed significantly different when both the p-value and adjusted p-value (Benjamini-Hochberg when multiple testing was required) padj (or Q) < 0.05. Genes defining each CM subtype were identified among those expressed in at least 10% of nuclei in either of the two groups of CM subtypes and visualized using the dittoDotPlot function in the dittoSeq package v1.6.0 [57]. In the analysis, adjusted p-values were determined using the Seurat function 'FindAllMarkers' through the Wilcoxon Rank Sum test. In the differential expression analysis, DEGs were identified by fitting a glmQLF (generalized linear model with a quasi-likelihood F-test). R v4.1.2 and Prism v9.4.0 were employed for statistical analyses.

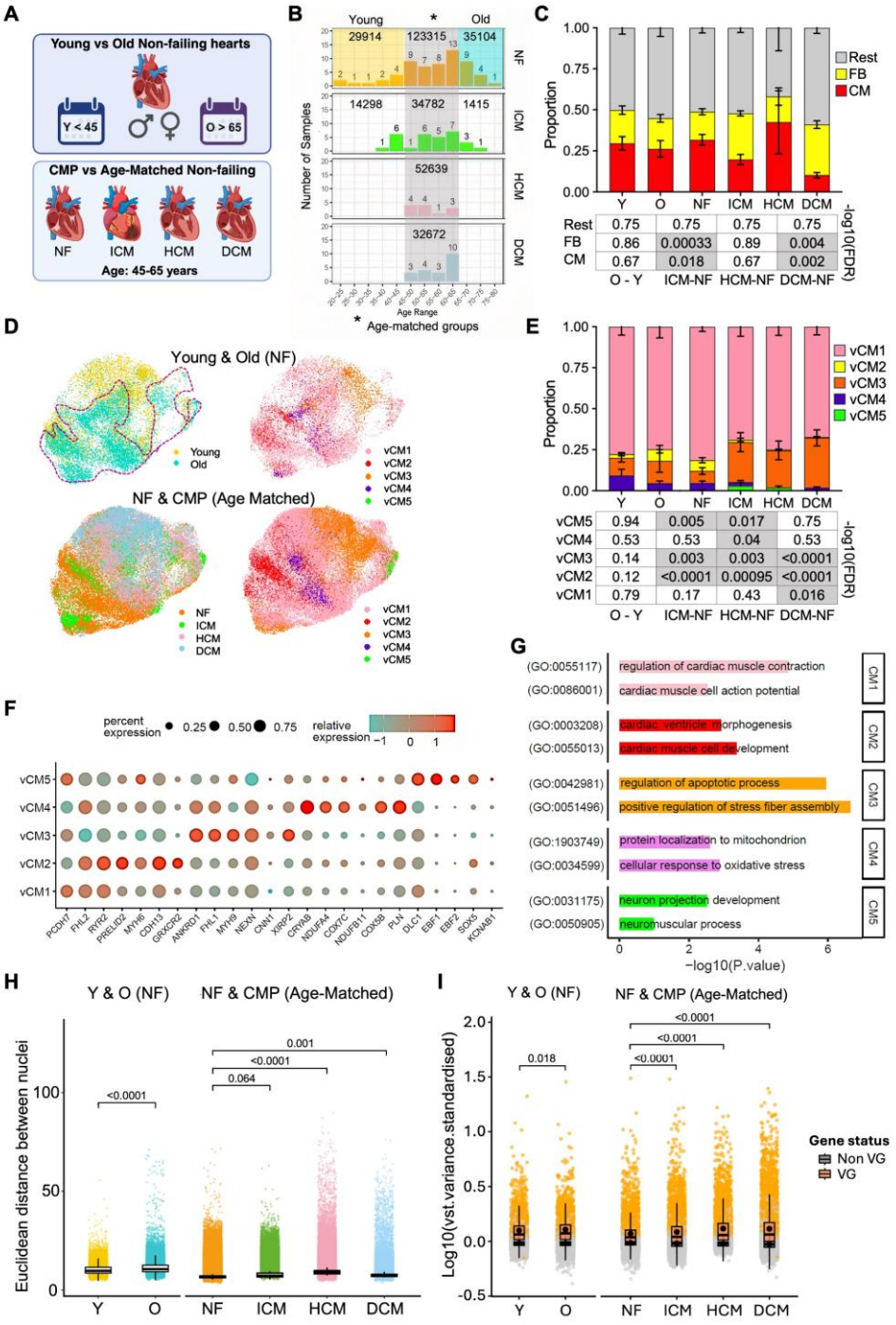


**Figure 1. Human single nuclear transcriptomics (10x) in aging and CMP. (A)** Comparison of Old (O) vs. Young (Y) groups in NF hearts (top) and in the HF samples including ICM, HCM, and DCM versus NF hearts in the age-matched groups from 45 to 65 years (bottom). **(B)** Histogram showing number of samples for each condition with number of samples of each age and the number of nuclei per group indicated. **(C)** Comparing CM, FB and the remaining cardiac cell type proportions across age groups and pathological conditions. The cell types proportions were compared between groups using Wilcoxon rank-sum tests. **(D)** UMAP of the CM nuclei and their subpopulations per age group and CMP etiology versus NF hearts. **(E)** Alterations in CM sub-population proportions in the different age groups in NF hearts and in the CMPs vs. NF hearts in the age-matched groups. Then subtype proportions were compared between groups using Wilcoxon rank-sum tests. **(F)** DEGs in CM nuclei sub-populations. **(G)** Top two associated enriched pathways of the DEGs per CM nuclei subpopulations. **(H)** Cellular heterogeneity among CM nuclei was quantified by Euclidean distance between nuclei. Statistical comparisons were performed at the nucleus level for Y versus O NF hearts and at the donor level for age-matched NF versus CMP groups using the Wilcoxon rank-sum test. **(I)** Gene-expression

variability was assessed using the top 2,000 highly variable genes identified in the merged dataset. Gene-wise vst.variance.standardized values were recalculated for each comparison group. For Y versus O NF hearts, variance and statistical comparisons were based on all nuclei within each age group, whereas for age-matched NF versus CMP groups, variance was recalculated per donor and compared using the Wilcoxon rank-sum test.

**Data availability statement**

RNA-seq and the integrated snRNA-seq data from all the studies have been deposited in GEO under accession number GSE284247.

## RESULTS

### Cardiomyocyte abundance and sub-clusters/states are altered in aging and disease

From 5 snRNA-Seq datasets [17-20, 22] (Table 3), we investigated gene expression and cell type changes associated with aging (in the absence of reported disease; non-failing (NF) aging) and with CMP, the latter being compared to age-matched NF controls. This integrated dataset included samples from young (Y; <45 (10)), NF old (O; >65 (14)), cardiomyopathic (ICM (19), HCM (12), and DCM (20)) and age-matched non-failing controls (37) (aged 45 - 65) (Fig. 1A, B) as well as Y (7) and O (4) samples with ICM. The integrated human dataset comprised 1,323,471 cardiac nuclei including 324,139 CMs and 265,369 FBs, which were from 123 individuals (15 in-house and 108 from 4 published datasets; Table 3) (Fig. 1B) [17-20, 22].
Details of the sex and age of these samples as well as of the CM nuclei contribution, QC metrics, sequencing platform, and library chemistry across studies and conditions are provided in the supplements (Supplementary Fig. 1 and 2, Table 3).

CM number as a proportion of total cardiac nuclei was lower in ICM and DCM relative to NF (Fig. 1C). FB nuclei present in this same integrated dataset were however significantly greater in ICM and DCM versus NF (Fig. 1C). No significant differences were detected between Y and O or in HCM. Consistent with the pattern of FB abundance across conditions detected in the snRNA-Seq data, RT-qPCR gene expression analysis in 291 LV tissue samples from our in-house collection (UZ/KU Leuven Biobank), revealed no difference in fibrotic marker gene expression with age but a greater expression in ICM and DCM (Supplementary Fig. 3A). After integration and clustering, CM nuclei were projected onto the five CM substates described in the Human Cell Atlas [20] (Fig. 1D), and their relative abundance and defining marker genes and gene ontologies determined (Fig. 1E-G). Seurat prediction scores confirmed mapping of all 5 CM states onto HCA clusters (Supplementary Fig. 4 and Supplementary File 2). Supporting successful sample integration, nuclei from all studies were represented in each CM cluster (Supplementary Fig. 5). The predominant CM subcluster 1 (vCM1) is enriched for *RYR2* and GO pathways specialized in cardiac muscle contraction and action potential. vCM2 like vCM1 is enriched for expression of *FHL2* and *RYR2,* increased expression of *PRELID2* (mitochondrial function [58] and of *MYH6* (cardiac contraction) and *CDH13* (cardiovascular protection) [59, 60]. vCM3 is enriched for expression of genes involved in stress responses, such as the transcription factor Ankyrin repeat domain-containing protein 1 (*ANKRD1*; AKA CARP) and *FHL1* [61, 62], which interact with myofilaments implicated in various CMPs and have been associated with cardiac arrhythmias. The minor, vCM4 sub-cluster is characterized by the expression of nuclear-encoded mitochondrial genes (*NDUFB11*, *COX7C, COX5B*) and *CRYAB*, encoding a cytoprotective heat shock protein that are consistent with high energetic demand/oxidative-stress resistance [63]. vCM5 represents a rare population of cells with a unique expression of the Rho GTPase activating protein *DLC1* and the *EBF2* transcription factor, as well as genes typically detected in neuronal lineages [64], such as *SOX5* and *KCNAB1* (Fig.1 F, G; Supplementary File 3). Highlighting changes in their gene expression in pathology, the proportions of nuclei populating each CM substate (vCM1-vCM5) varied with etiology (Fig. 1D-G). Most notably, the proportion of vCM2 was lower and vCM3 greater in CMP samples relative to age-matched NF controls. The more minor vCM4 was significantly lower in HCM while vCM5 was elevated in ICM and HCM relative to proportion in NF. No statistically significant differences in proportions of vCM states were detected between Y and O NF CM samples. Disease and aging are also associated with transcriptional dysregulation leading to increased variance of expression of genes and/or increase in cell-cell variability [12]. CM heterogeneity (Euclidean distances (EDs)) between CM nuclei was greater in O than in Y (Fig. 1H, Supplementary file 4), as well as in CMPs in comparison to their age-matched NF samples, which was particularly evident in ICM and HCM (Fig. 1H). The variance in expression of the top 2,000 variable genes was also significantly increased with aging ($p = 0.031$, Fig. 1I), and in CMPs (Fig. 1I; Supplementary File 5). Notably, *PLCG2*, *NPPB*, and *MYL7* exhibited a greater level of expression variance in O versus Y CM but lower variance in CMP CMs versus age-matched NF CM (Supplementary File 5).

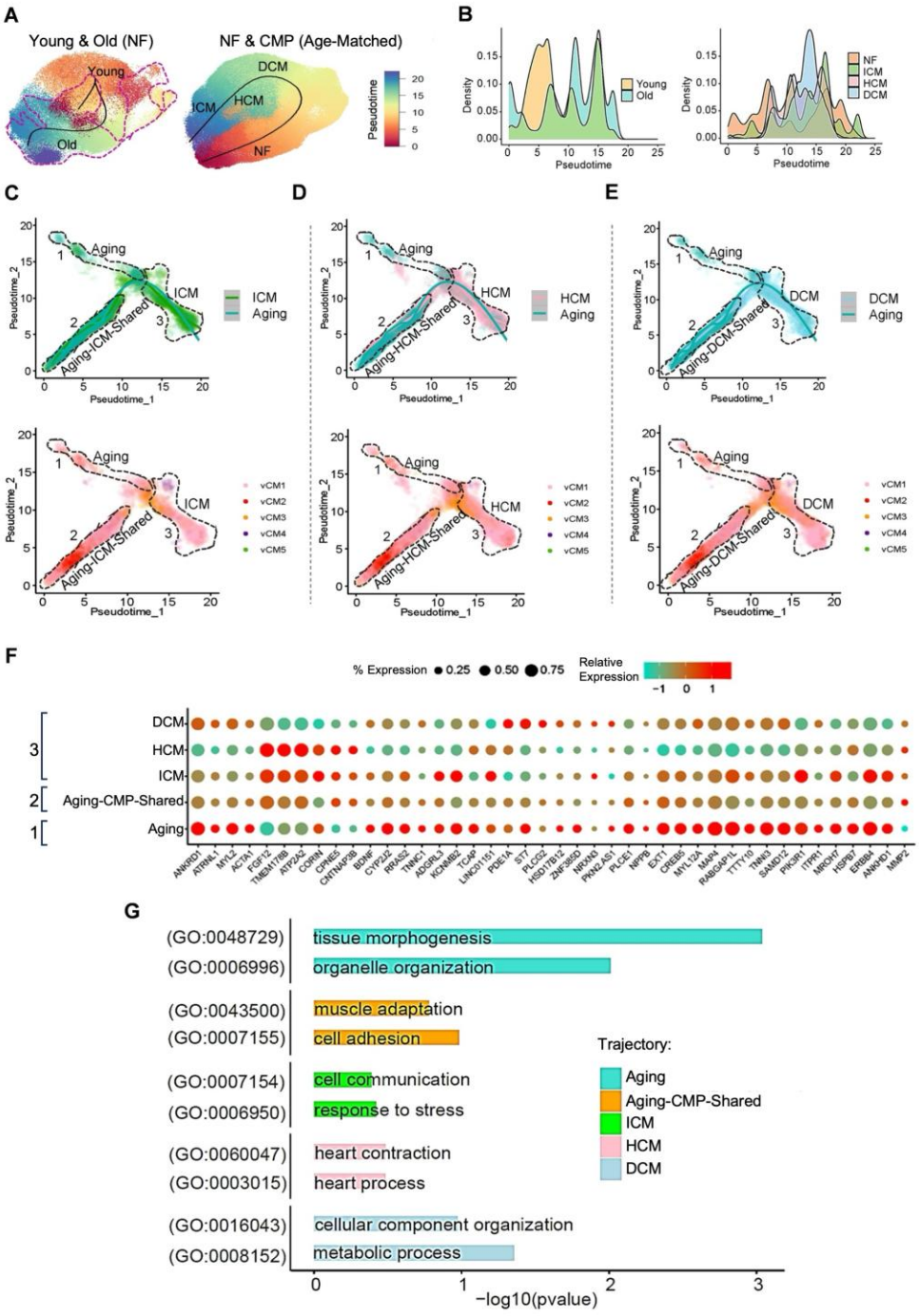


**Figure 2. Cell state ordering of CM nuclei transcriptomes in human aging and CMPs. (A)** Slingshot trajectory analysis of the transcriptome alteration by aging in NF hearts and CMP vs NF hearts in the age-matched groups. **(B)** Frequency of the nuclei across the calculated pseudo-times of the analysis. The ordering of CM state transcriptomes of each condition are indicated by the colours indicated. Averaged trajectories are additionally shown. **(C-E)** Ordering of the aging and CMP. CM nuclei transcriptomes between states. The first path is a representation of the ordering of CM in NF hearts; the second trajectory shows the overlap of the NF and CMP CM transcriptomes. The third path refers to the distinct ordering of transcriptomes of each CMP. The top row shows the aging (NF) and CMP CM nuclei; the bottom row shows the CM subpopulation distributions across the trajectories. **(F)** Enriched genes in aging (NF) and each CMP across their exclusive and shared trajectories. The trajectories identified in C-E are indicated on the left of the condition. **(G)** Pathways associated with DEGs in the transcriptome trajectories.

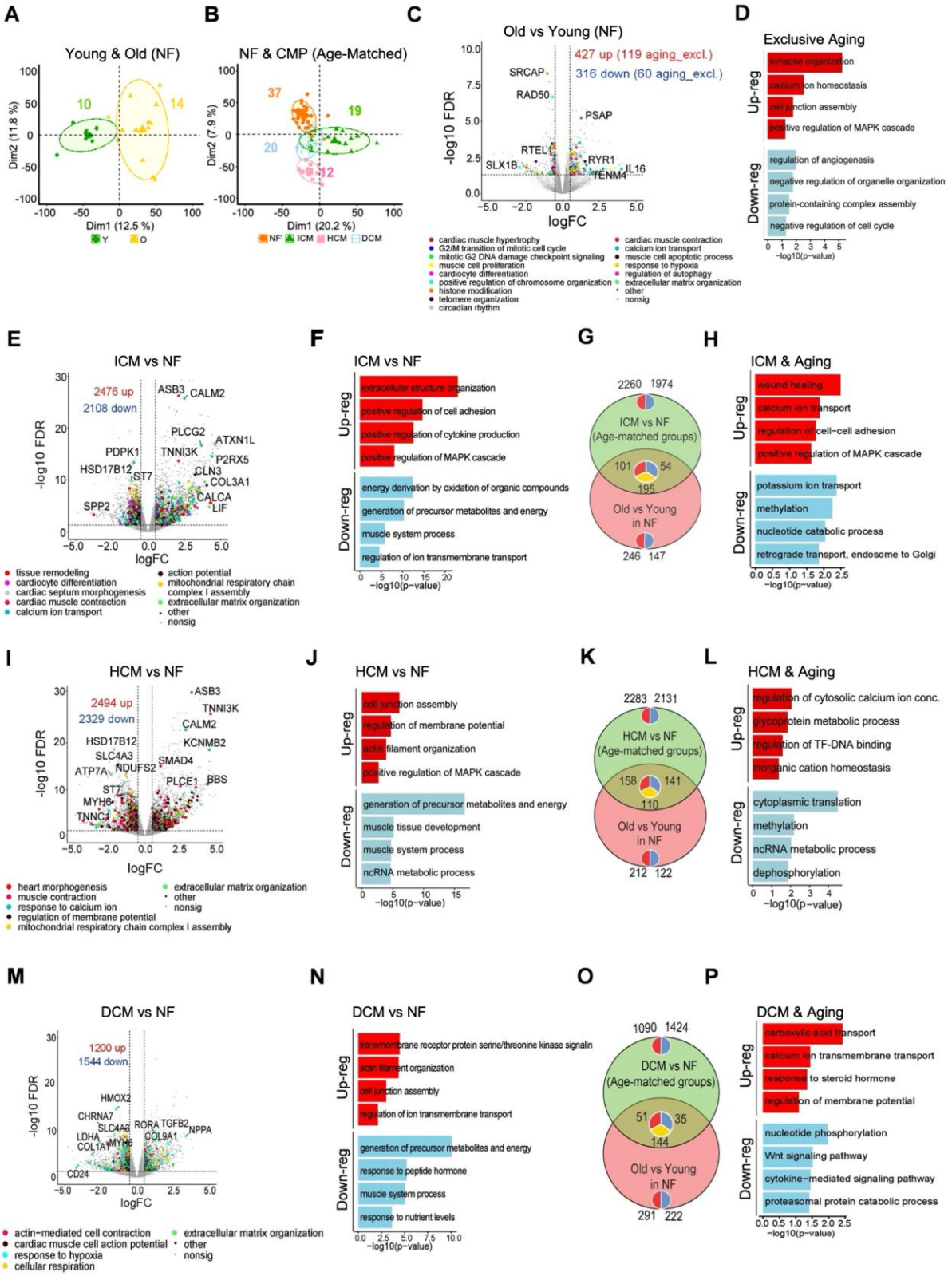


**Figure 3. Comparisons between aging and CMPs in human (Pseudobulk data, derived from snRNA-Seq datasets). (A)** Principal Component Analysis (PCA) of Y vs O NF heart CM transcriptomes. **(B)** PCA of the cardiomyopathies and NF hearts in the age-matched groups. **(C)** DEGs identified in O vs Y in the CM nuclei from NF hearts. **(D)** Enriched pathways of DEGs exclusively in O vs Y. **(E)** DEGs in ICM versus NF hearts in the age-matched group. **(F)** Top enriched pathways of the DEGs

in ICM vs NF. **(G)** Shared and distinct DEGs in aging in NF and ICM vs NF. H) The top enriched pathways of the shared DEGs in ICM vs NF and aging in NF hearts. **(I)** DEGs in HCM vs NF in the age-matched group. J) Top enriched pathways of the DEGs in HCM vs NF. **(K)** Shared and distinct DEGs in aging in NF and HCM vs NF. L) Top enriched pathways of the shared DEGs in HCM vs NF and aging in NF. **(M)** DEGs in DCM vs NF in the age-matched group. **(N)** Top enriched pathways of the DEGs in DCM vs NF. **(O)** Shared and distinct DEGs in aging in NF and DCM vs NF. **(P)** Top enriched pathways of the shared DEGs in DCM vs NF and aging in NF hearts. In the Venn diagrams, red and blue small circles indicate consistently up- or downregulated DEGs; yellow marks shared DEGs with opposing regulation between comparisons.

**Cross-sectional transcriptomic manifold analysis reveals shared and distinct CM states in aging and cardiomyopathy**

To explore whether aging- and CMP-associated CM states exhibit regions of overlap along pseudotime trajectories between different states, we performed Slingshot analysis on cross-sectional snRNA-seq profiles. While this analysis primarily infers transcriptomic manifolds and relative cellular-state ordering when performed on cross sectional data, it can also be used to infer temporal progression or lineage relationships between states. When applied separately to Y versus O NF CM and to NF versus ICM, DCM, or HCM comparisons, this analysis identified condition-associated gradients of gene expression across the inferred manifolds (Fig. 2A, B). In the combined dataset of all conditions, aging- and CMP-associated CM states showed both overlapping and condition-enriched regions of transcriptomic state space (Fig. 2C-E).

Marker genes expressed across the three main inferred trajectory branches reflected both shared and distinct transcriptional features of aging and CMP (Fig. 2F). Genes enriched along the aging-associated branch were associated with heart tissue morphogenesis and organelle organization, including *TNNI3* and *MAP4*. In contrast, genes enriched in regions occupied by both aging- and CMP-associated nuclei were related to muscle adaptation and cell adhesion, including *TNNT1*, *MYH7*, *VCL*, and *CTNND2*. Branches enriched for ICM, HCM, and DCM nuclei were associated with responses to stress, heart contraction, and metabolic processes, respectively (Fig. 2G; Supplementary File 6). These findings support partial overlap between aging- and CMP-associated CM transcriptional states.

**DEG and associated pathways in aging are distinct but show overlap with cardiomyopathies**

We next identified DEGs that were specific to or shared between aging and each CMP. To this end, we performed a pseudo-bulk analysis of aggregated datasets of raw gene expression, which mitigates impact of intra-sample cellular variation and data sparsity [33]. Principal component analysis (PCA) separated samples by etiology and age (Fig. 3A, B). Since sex distribution was not fully balanced across all disease groups (Supplementary File 7), it was included as a covariate in donor-level pseudobulk analyses where model design permitted. Between Y and O, 427 genes were upregulated and 316 downregulated (Fig. 3C). These genes were related to processes including cardiac muscle cell hypertrophy, histone modifications, G2/M transition of the mitotic cell cycle, cardiac muscle cell contraction, calcium ion transport, response to hypoxia, and ECM organization (Fig. 3C). To exclude disease-related genes from the collection of genes differentially expressed between Y and O and to identify a geneset related to aging in NF CM, genes that were also differentially expressed in ICM, DCM and HCM, were subtracted. Between Y and O, 119 genes were exclusively elevated in expression and 60 exclusively showed lower expression. Genes with higher expression were associated with cell junctions (*CNTNAP2*, *CDHR3*), calcium homeostasis (*CALR*, *TNNI3*), and the MAPK pathway/growth factor signaling pathway (*NRG1, IGF1R*), while genes with lower expression were linked to angiogenesis (*MAPK7, ADAMTS1*) and the cell cycle (*PPP1R10, BRINP3*) (Fig. 3D; Supplementary File 8).

In comparison with NF, ICM CM showed extensive transcriptional remodeling with 2476 genes upregulated and 2108 downregulated (Fig. 3E; Supplementary File 9). Upregulated genes were enriched for tissue remodelling, ECM organization, calcium transport, cell adhesion, cytokine production, and MAPK signaling, including *MMP14*, *COL1A2*, *CALM2*, *COL3A1*, *SMAD4*, *DAB2*, *MIF*, and *MAP3K10* (Fig. 3F). Downregulated genes were linked to cardiac contraction, mitochondrial function, energy production, and muscle-cell processes, including *RYR2*, *ATP1A2*, *NDUFAF4*, *PFKM*, *NDUFA12*, and *MYH7*. Of the ICM DEGs, 101 upregulated and 54 downregulated genes overlapped with aging (Fig. 3G), with shared pathways being involved in wound healing, calcium transport, cell-cell adhesion, MAPK signaling, potassium transport, and methylation (Fig. 3H; Supplementary File 9). ICM-specific pathways included T-cell activation and cytokine production among upregulated genes, and membrane-potential regulation and metabolic energy processes among downregulated genes (Supplementary Fig. 6A; Supplementary File 9).

HCM CM showed broad transcriptional remodeling in comparison to NF, with 2494 genes upregulated and 2329 downregulated (Supplementary File 10). These genes were associated with heart morphogenesis, muscle

contraction, and membrane-potential regulation (Fig. 3I). Genes specifically upregulated in HCM were enriched for cell-junction assembly, action potential regulation, filament organization, MAPK signaling, and calcium signaling, whereas downregulated genes were involved in metabolism, muscle tissue development, ncRNA metabolism, histone methylation, and splicing (Fig. 3J; Supplementary Fig. 6B; Supplementary File 10). Of these DEGs, 158 upregulated and 141 downregulated genes overlapped with aging (Fig. 3K; Supplementary File 10). Shared HCM-aging genes were associated with cytosolic calcium regulation, glycoprotein metabolism, transcription factor DNA binding, ncRNA metabolism, methylation, and dephosphorylation, including *PLCG2*, *RYR1*, *METTL17*, and *PHF1* (Fig. 3L).

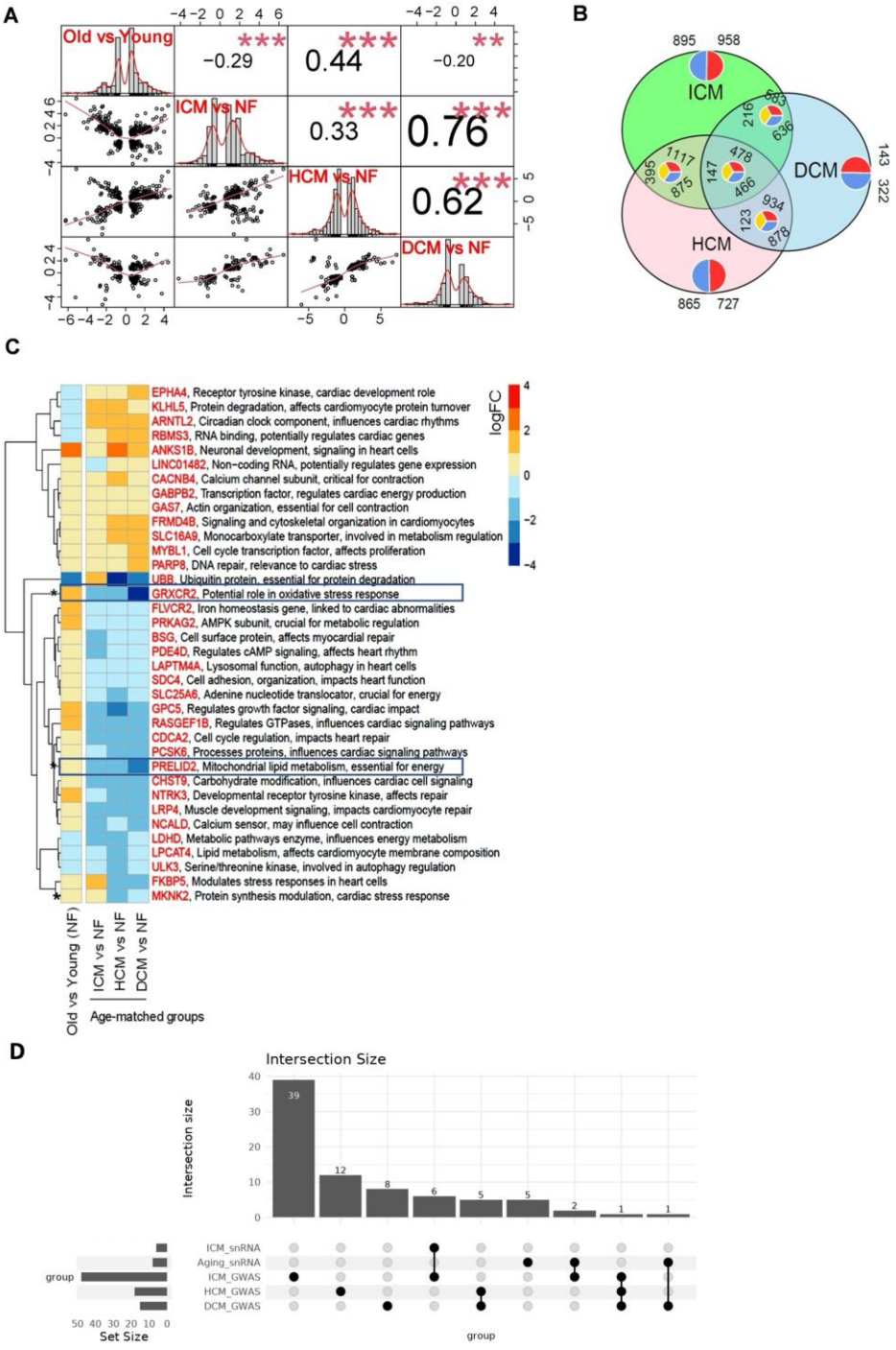

**Figure 4. Correlation between aging and CMP transcriptomes in human and relation to disease-related SNPs. (A)** Spearman's Rank-Order correlation based on the total detected DEGs in the comparisons. **(B)** Shared and exclusive DEGs in the CMPs vs NF hearts in the age-matched groups. **(C)** Expression heatmap of DEGs shared between aging and CMPs (aggregated gene expression values > 100, taken from every nucleus within each sample). In the Venn diagram, red and blue indicate consistently up- or downregulated DEGs; yellow marks shared DEGs with opposing regulation between comparisons. **(D)** UpSet summary plot of the integrated GWAS/eQTL resource and snRNA-Seq data in aging and cardio pathology.

In the comparison between DCM and NF, 1200 genes were upregulated and 1544 downregulated (Fig. 3M; Supplementary File 11). These DEGs were mainly associated with hypoxia response, cellular respiration, and ECM organization (Fig. 3M). DCM-specific upregulated genes were enriched for receptor serine/threonine kinase signaling, actin-filamin organization, cell-junction assembly, and TGF-β signaling, whereas downregulated genes were linked to energy metabolism, peptide-hormone responses, muscle-system processes, and vascular-associated pathways (Fig. 3N; Supplementary Fig. 6C; Supplementary File 11). Of the DCM DEGs, 51 upregulated and 35 downregulated genes overlapped with aging (Fig. 3O; Supplementary File 11) with pathways involving calcium transport, steroid-hormone response, membrane-potential regulation, Wnt signaling, and protein catabolism being shared between these groups (Fig. 3P).

To control for influence of each study on the results of the integrated analysis, we performed a leave-one-study-out sensitivity analyses using donor-level pseudo-bulk CM profiles (Supplementary Figs. 7, 8; Supplementary Files 7, 12, and 13). Importantly, Log-fold changes from the analysis model including all datasets were generally concordant with those obtained after excluding individual studies, indicating that the main transcriptional signatures were not solely driven by a single source dataset (Supplementary Fig. 7). However, notable effects were detected. For those genes lost from the list of DEG upon removal of one study, more than half were recurrent amongst those lost for each study excluded (52% in DCM, 62% in HCM, 80% in ICM and 70% in Y vs O) (Supplementary Fig. 8). Since these genes primarily showed the lowest fold change or FDR (Supplementary Files 12, and 13), their loss from the DEG of the complete dataset is consistent with a reduction in power for their detection at statistical significance. Genes gained due to exclusion of a particular dataset showed a different pattern, likely reflecting specific features of the dataset removed including donor composition, age/sex balance and etiology (Supplementary File 7).

**HCM, ICM and DCM exhibit unique differentially gene expression profiles that vary in their strengths of correlation with each other and with aging.**

Having identified genes and pathways altered in each CMP and how they overlapped with aging, we next probed more deeply the genes specific to each condition and the strengths of overlaps between each etiology, as well as with aging. The aging-associated transcriptome showed a stronger correlation with HCM (r = 0.44) than with ICM and DCM, where weaker negative correlations were observed (r = -0.29 and -0.20 respectively) (Fig. 4A). Among the CMPs, the highest correlation was observed between ICM and DCM (r = 0.76), followed by DCM and HCM (r = 0.62). However, DEG overlap analysis revealed that ICM and HCM shared the largest number of dysregulated genes (1117 upregulated and 875 downregulated genes), with an additional 478 upregulated and 466 downregulated genes commonly altered across all three cardiomyopathies, including DCM (Fig. 4B). Shared upregulated DEGs across the CMPs, excluding aging, were enriched for regulation of membrane potential, and actin filament organization, while shared downregulated genes were associated with cellular respiration, the electron transport chain, and muscle contraction (Supplementary Fig. 6D; Supplementary File 14). The enrichment of differentially expressed genes involved in cardiac excitation contraction coupling and glycolysis in ICM and to a lesser extent in DCM and HCM and their near absence in aging, is clearly observed in a heatmap showing expression of selected ion channel, calcium handling and metabolic genesets (Supplementary Fig. 6E, F). With the aim of more clearly identifying distinguishing features of (biomarkers) of CM HF and aging, we next probed for genes that were highly expressed (>100 reads), as well as being differentially expressed in relation to their comparator (Fig. 4C). Genes that were not differentially expressed in any condition were excluded. This analysis revealed 36 genes that were either altered in the same direction in each CMP and aging, down in aging and up in each CMP or up in aging and down in each CMP (Fig. 4C). For a few genes, ICM showed a different pattern to HCM and DCM, showing either concordance with aging and not HCM and DCM (*FKBP5* and *MKNK2*) or discordance with aging, HCM and DCM (*UBB*, upregulated; *LINC04182*, downregulated). To determine whether these DEGs are related to CM biology, we examined their cell-type specific expression in the Human Cardiac Cell Atlas (Supplementary Fig. 9A, B). *PRELID2,* encoding a protein involved in phosphatidic acid transfer located to

the mitochondrial intermembrane space was exclusively expressed in CM, *GRXCR2*, predominantly in CM but also in adipocytes. *CDCA2*, *LINCO1482*, *CHST9* and are also enriched in CM but show expression in other cardiac cell types.

Overlaps in transcription responses between aging and CMP were further examined by RT-qPCR analysis of classical biomarkers of cardiac remodeling and stress performed on samples spanning the study groups analysed in our in-house cardiac tissue (LV) collection (UZ/KU Leuven Biobank) and the Human Heart Tissue Biorepository at the University of Pennsylvania (Supplementary Fig. 3B). This analysis revealed strong induction of hypertrophic markers (*NPPB, NPPA, XIRP2* upregulated; *MYH6* downregulated), fibrotic markers (*COL1A1, POSTN*), and the senescence marker *GLB1* (encoding the senescence marker b-galactosidase) in ICM and DCM, but not in HCM. In aged tissue, *MYH7* expression was specifically increased (Supplementary Fig. 3B).

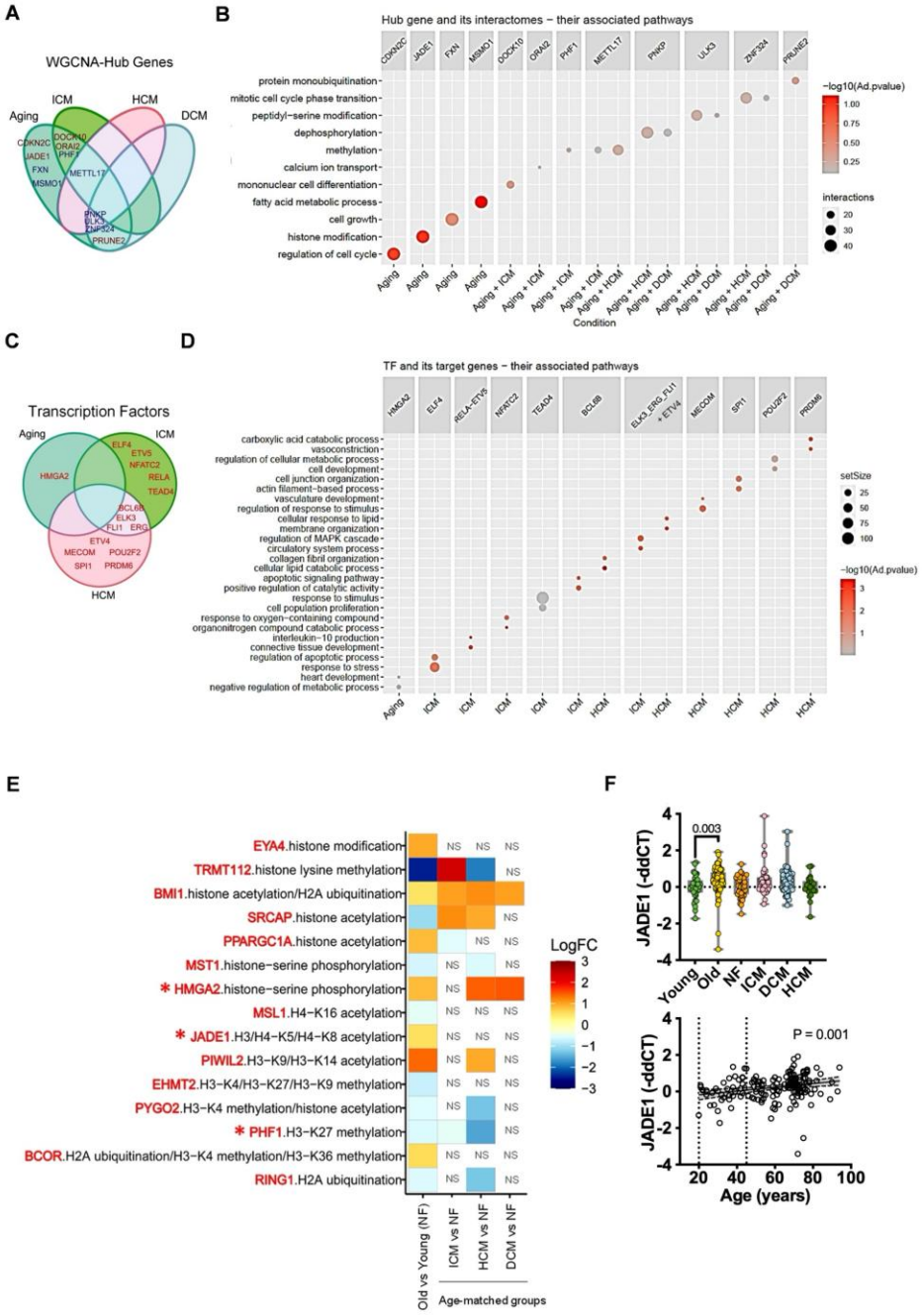


**Figure 5. Identification of hub co-expressed genes and candidate regulatory drivers in NF aging and their overlap with CMPs**. **(A)** Hub co-expressed genes in the aging process and their overlap with pathologies

indicated by Weighted Gene Co-expression Network Analysis (WGCNA), red and blue gene labels represent up- and down-regulated genes, respectively. **(B)** Pathways associated with each hub gene and their interactome. **(C)** Upregulated TFs with motifs identified in upregulated genes in aging and CMPs. **(D)** Top two pathways associated with upregulated TFs and their target genes in aging and CMP. **(E)** Differentially Expressed epigenetic factors contributing to gene regulation, with asterisks indicating them as candidate hub gene/TFs as drivers of NF heart aging and CMPs in A and B, NS=nonsignificant. **(F)** Experimental validation for JADE1 expression in aging and the left ventricular tissue samples from the CMPs shown by qPCR.

**Comparison of gene expression changes between aging in NF hearts and aging with ICM identifies candidate nodal regulators of disease and health**

To complement the identification of CM markers of disease or aging in NF hearts through exclusion of disease-related genes from genes differentially expressed with aging, we performed an additional analysis, whereby we compared DEG associated with aging in NF CM (no reported pathology) with those in ICM that were altered between O with ICM (>65) vs Y with ICM (<45) (Fig. 1B). This age-stratified ICM analysis included 7 Y ICM, and 4 O ICM samples. With the inclusion of this additional older ICM group, we aimed to also gain insight into the interaction between age and ICM in the development of HF. Within ICM, we identified 1,306 DEGs, of which 232 were significantly upregulated and 1,074 downregulated (Supplementary Fig. 10A; Supplementary File 15). Consistent with a metabolic shift in older ICM hearts [65], genes involved in disrupted glycogen metabolism were particularly enriched, including *GCK* and *PYGL,* which were upregulated. Genes involved in chromatin remodeling and histone modification exhibited significant changes with aging in ICM. Of note, histone deacetylases that act to repress gene repression [66], including HDACs, and SIRT2, exhibited notably lower expression in older ICM samples than in Y. Genes linked to cardiac hypertrophy and structural integrity [67], such as nuclear lamina-related *MLIP* and *LMNA,* transcription factors *GATA4, GATA6 HAND2* and *MEF2A,* adaptor protein and cytoskeletal related *SORBS2,* were also consistently lower in expression in O than in Y ICM samples.

An additional prominent feature of the aging ICM transcriptome, was the downregulation of genes associated with adrenergic (*ADRA1A*) and $Ca^{2+}$ signaling, particularly of the machinery governing sarcoplasmic reticulum $Ca^{2+}$ release and cytosolic $Ca^{2+}$ clearance (*PLN, ATP2A2, RYR2, JPH2, SLC8A1, CASQ2* and *TRDN)* [13]. *CAMK2D,* which regulates $Ca^{2+}$ channels was also downregulated. *ATP1A2,* which governs membrane potential was downregulated with aging while the $Ca^{2+}$ activated BK channel, *KCNMA1* and *ITPR3* were upregulated.

To identify the genes associated with aging in the CM from NF hearts vs those identified in the comparison between CMP and age-matched controls, DEG identified in a comparison between Y and O ICM CM were intersected with DEG identified in NF O vs Y CM. This analysis identified a subset of 42 overlapping DEGs, of which 29 were upregulated and 13 downregulated (Supplementary Fig. 10B and C). Among these, *HMGA2, ORAI2, KCNQ2, CNTNAP2, SLC24A2,* and *NRG1* were upregulated in NF and ICM aging CM, suggesting they either act as nodal regulators predisposing aged hearts to ICM or represent general markers of aging. In contrast, other upregulated DEGs, including *IGF1R, SMAD7, HSPA5, BMPR1A, IRS2, CDKN2C, FNIP2, MMP2, PALMD,* and *TNNI3* were uniquely altered in aging NF CM (not in ICM) (Supplementary File 15).

**Aging and cardiomyopathy DEGs overlap with GWAS/eQTL signals for non-congenital CVDs**

To explore whether age-related CM transcriptional remodeling included genes identified as CVD-associated loci, we intersected aging-associated DEGs with GWAS identified loci. We assembled an integrated GWAS-eQTL dataset for non-congenital CVD traits and compared it with DEG from our CM snRNA-seq analysis. Directional concordance was defined as matching directions between eQTL effect and expression change (i.e. risk↑expr with an upregulated DEG, or risk↓expr with a downregulated DEG). For CMP, concordance additionally required that the GWAS trait class matched the clinical condition.

Using the UpSet summary (Fig. 4D; Supplementary File 16), the integrated GWAS/eQTL resource comprised 48 genes for ICM, 18 for HCM, and 15 for DCM. Overlaying these with aging DEGs revealed three loci where age-linked expression changes aligned with CVD risk: FCHO1 (rs73015714) and FUT11 (rs3812637), both upregulated with age and carrying risk↑expr eQTLs associated with ICM, and NMB (rs1051168), downregulated with age and carrying a risk↓expr eQTL linked to DCM. Thus, a small subset of age-related CM transcriptional changes occurred at loci previously implicated in non-congenital CVD risk.

We next examined CMP DEGs for concordance with their respective GWAS sets. In ICM, six loci met the directional concordance criterion: APOB (rs585967), CYP21A2 (rs3130683), EXOSC5 (rs2241713), RNF215 (rs6006426), TBX20 (rs6963934), and TCF21 (rs12190287). No concordant overlaps were detected for HCM or DCM at this stringency. Together, these overlaps

provide supportive genetic annotation for a subset of aging- and CMP-associated transcriptional changes and highlight candidate loci for future functional follow-up.

**Hub genes and regulatory networks linking aging to cardiomyopathies**

To uncover gene regulatory hubs in aging and CMPs, we applied two complementary approaches: 1. Weighted gene co-expression network analysis (WGCNA) using DEGs specific to aging and those shared with ICM, HCM, or DCM, and, 2. Transcription factor (TF) motif enrichment on the full set of DEGs across aging and CMPs to maximize gene coverage and analytical precision (Fig. 5A-D; Supplementary Figs. 11-13; Supplementary File 17-19). Among the upregulated DEGs exclusive to aging, *CDKN2C* encoding p18-INK18c, which is an inhibitor of the cyclin dependent kinases CDK4/6, and JADE1, which is involved in histone acetylation, DNA replication, and cell growth, were identified as candidate hub genes.

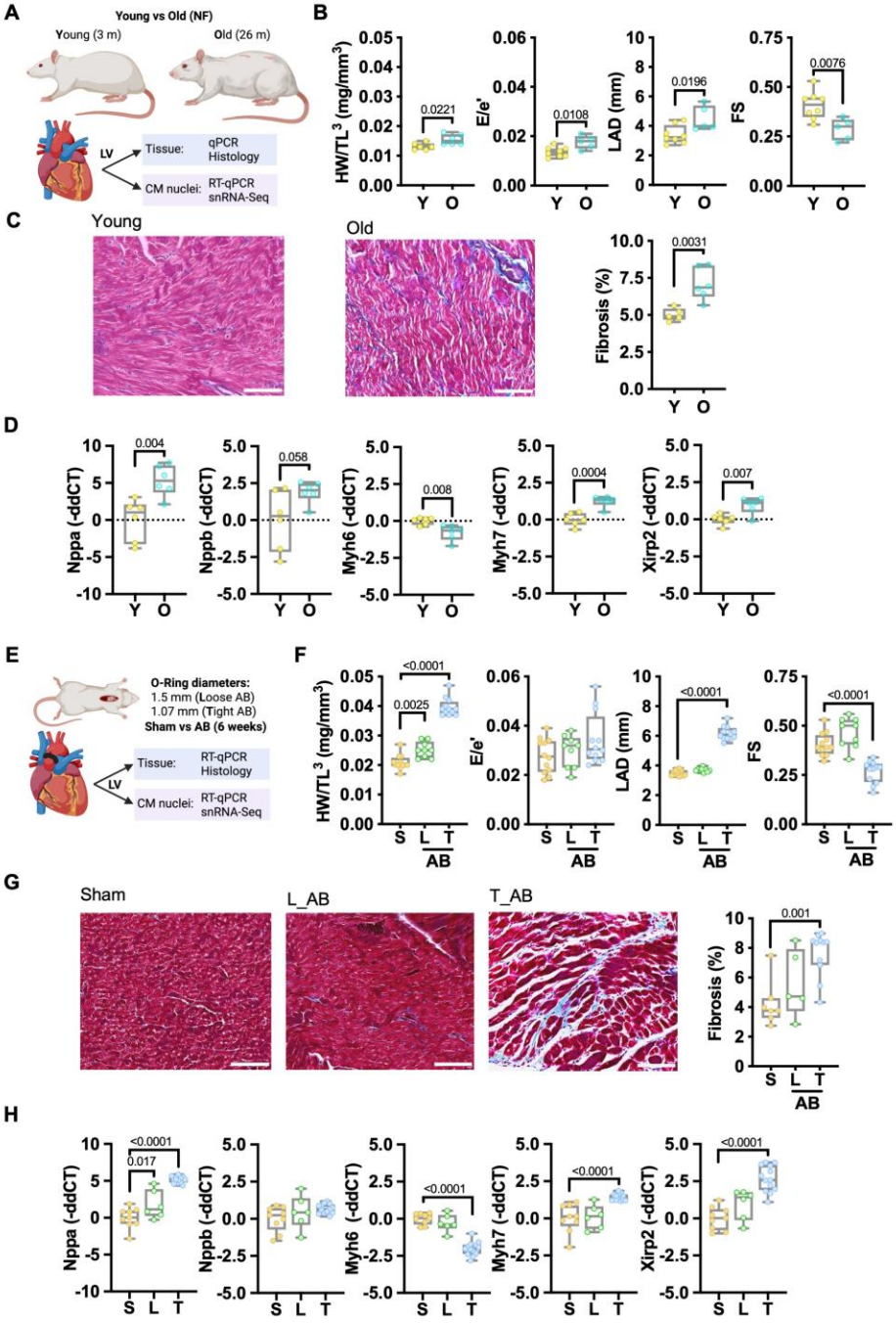

**Figure 6. Cardiac remodeling during aging and in response to pressure overload in rats. (A)** Schematic of aging experiment. **(B)** Parameters of cardiac remodeling as shown. T-test. **(C)** Histological analysis of fibrosis by Masson trichrome staining. Left, example images and right, quantitation of % fibrotic area. t-test. Scale bar = 50 µm. **(D)** RT-qPCR analysis of markers of cardiac stress performed on LV tissue mRNA. t-test. **(E)** Schematic of experiment to test effect of pressure overload (AB) on cardiac remodelling. The diameter of the O-ring used to induce a mild (Loose, L; 1.5 mm) and severe (tight, T; 1.07 mm) stenosis is shown. The band is place but not sutured in Sham (S). **(F)** Parameters of cardiac remodeling as shown. One way ANOVA. **(G)** Histological analysis of fibrosis by Masson trichrome staining. Left, example images and right, quantitation of % fibrotic area. Scale bar = 50 µm. One way ANOVA. **(H)** RT-qPCR analysis of markers of cardiac stress performed on LV tissue mRNA. One-way ANOVA.

Conversely, *FXN* and *MSMO1*, with roles in cell growth and fatty acid metabolic processes, were downregulated (Fig. 5A, B; Supplementary File 17). Several DEGs shared between aging in NF CM and ICM were also identified as candidate hub genes. These include genes encoding the DOCK10 Rho GTPase and the store-operated $Ca^{2+}$ entry channel ORAI2, which were both upregulated. The PRC component, PHF1 [68], was downregulated (Fig. 5A, B; Supplementary File 17). Additionally, expression of the methyl transferase-like *METTL17* [69], was downregulated in both ICM and HCM, as well as in NF aging. This gene emerged as a hub in the gene-gene interactomes, suggesting a role in driving susceptibility to both ischemic and hypertrophic pathologies (Fig. 5A, B; Supplementary File 17). Furthermore, the dual kinase phosphatase *PNKP* (involved in DNA repair), *ULK3* (associated with peptidyl serine modification and autophagy), and *ZNF324* (linked to mitotic cell cycle transition) were all downregulated in aging, HCM, and DCM, suggesting roles in predisposing aged hearts to these pathologies. *PRUNE2,* involved in protein monoubiquitination was also detected as a hub gene of the upregulated co-expressed/interactome genes in aging and DCM [70] (Fig. 5A, B; Supplementary File 17).

To identify upstream transcriptional regulators of the DEGs, we screened for TFs whose motifs were enriched in promoters of DEG and that were themselves differentially expressed. These were designated as regulatory TFs. This analysis revealed TFs uniquely altered in aging, as well as TFs shared between ICM and HCM, but not DCM (Fig. 5C; Table 4; Supplementary File 18). No common regulatory TFs were detected between aging and the CMPs. Notably, the recognition motif of the non-histone chromosomal high-mobility group protein HMGA2 was specifically enriched in the promoters of the 50 most upregulated genes exclusive to aging NF CM (Table 4; Supplementary Fig. 13A; Supplementary File 19). Supporting a functional role, HMGA2 expression itself increased with age in NF. Although HMGA2 motifs were absent in HCM and DCM DEGs, HMGA2 expression was nonetheless elevated in both conditions (HCM and DCM vs. NF; Supplementary Fig. 13B; Supplementary Files 10, 11).

Overlap of motifs for upregulated TFs including those for BCL6B, ELK3, ERG, and FLI1 was also detected in genes upregulated in ICM and HCM (Fig. 5C; Table 4). In ICM, BCL6B targeted genes including *RHOC, ATP2A3, FLT4, PIK3R5,* and *GDNF* that were associated with cytoskeletal dynamics, calcium signaling, vascular development, neural development, PI3K–AKT signaling, and apoptosis (*SNAI2, GDNF, FCGR2B*) (Fig. 5D; Supplementary File 18). In HCM, the BCL6B motif was enriched on genes linked to lipid catabolism and fibril organization (Fig. 5D; Supplementary File 18).

In ICM, ELK3, ERG, and FLI1 targeted genes were involved in the MAPK cascade and circulatory system processes. In HCM, these TFs, together with ETV4, were associated with genes regulating cellular responses to lipids and membrane organization (Fig. 5D; Supplementary File 18). Additional TFs identified in HCM included MECOM, SPI1, POU2F2, and PRDM6, enriched on genes linked to vasculature development and stimulus response, actin filament-based processes and cell junction organization, cell development and metabolism, vasoconstriction, and carboxylic acid catabolism (Fig. 5C, D; Supplementary File 18). Conversely, the recognition motif of ATF3 was enriched among downregulated genes in both HCM and DCM, and ATF3 itself was also downregulated (Table 4).

Given the inclusion of epigenetic dysregulation as a 'Hallmark of Aging', including in the cardiovascular system [3, 71], we next investigated expression of components of the epigenetic machinery. GO term enrichment analysis revealed a number of epigenetic regulators differentially expressed in both aging and pathology (Fig. 5E). The exclusive aging-associated DEGs were *EYA4* (serine/threonine phosphatase [72]), *JADE1* (histone acetyltransferase, *HAT* [73]) and *BCOR* (involved in H3K4/H3K36 methylation [74]), while *MSL1* (involved in histone acetylation [75]) and *EHMT2* (histone methyltransferase [11]) were downregulated. Upregulation of *JADE1* in aging was detected by RT-qPCR analysis performed on RNA isolated from an independent collection of LV tissue (Fig. 5F). The altered expression of this complement of epigenetic modifiers, which would be associated with increased histone acetylation and reduced repressive methylation, would lead to a shift towards a more open chromatin, supporting

increased transcriptional activity. Upregulated in ICM, HCM, DCM as well as in aging was BMI1, a component of PRC1, which maintains histone H2A ubiquitination and gene silencing [76]. *PIWIL2*, associated with the regulation of chromatin state and piRNA-mediated gene silencing [77], was upregulated in aging and HCM but not in other conditions, implying a more specific role in promoting chromatin changes linked to hypertrophic adaptation. Other epigenetic factors altered exclusively in pathological conditions are shown in Supplementary Fig. 14. The functional roles of the transcriptional regulators identified were probed by integration of the co-expression network and transcription factor enrichment analyses. This analysis identified *JADE1*, *PHF1*, and *HMGA2* as candidate hub genes and key regulatory elements, as well as histone modifying proteins (Fig. 5E) involved in transcriptional remodeling during cardiac aging.

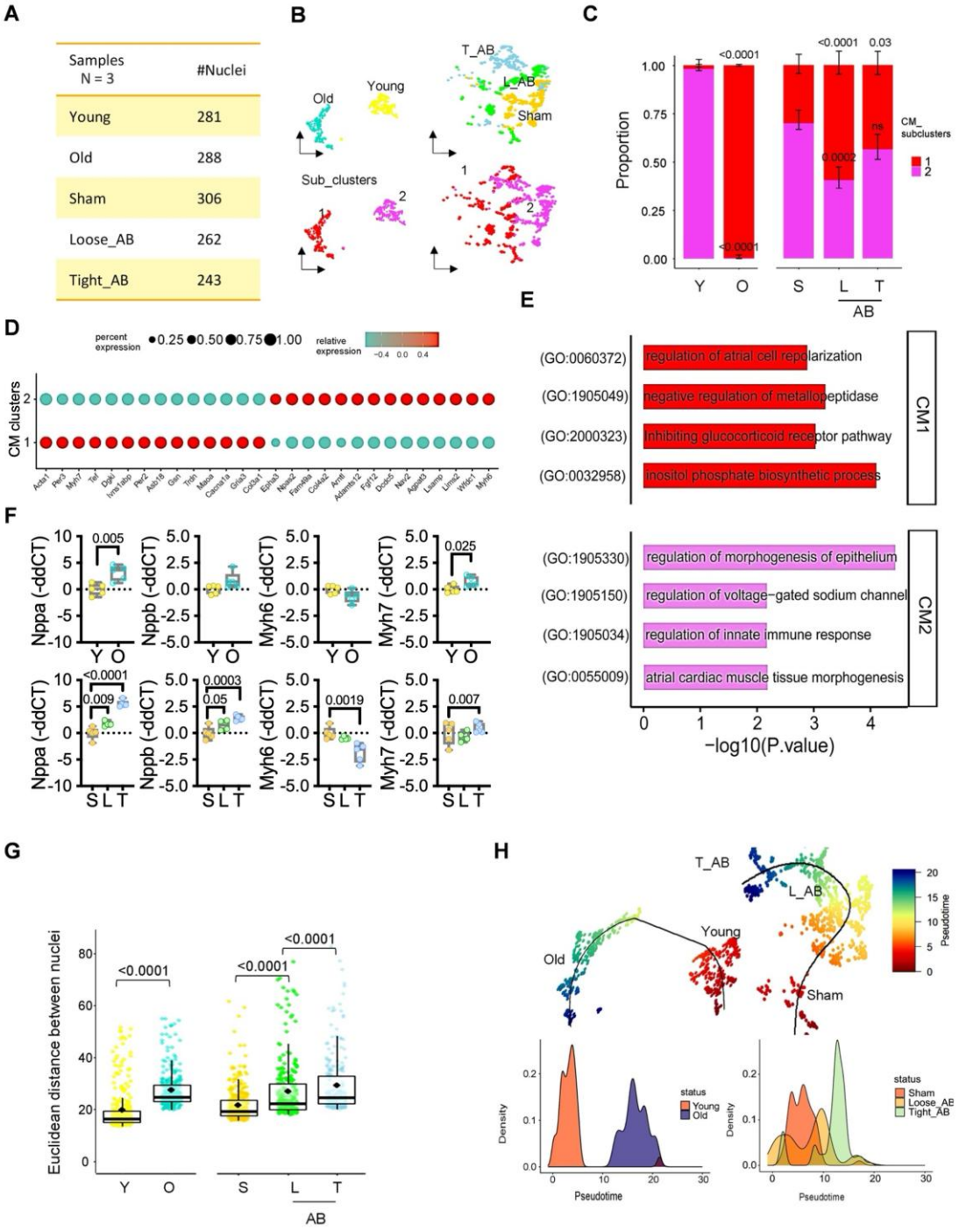

**Figure 7. snRNA-Seq analysis in aging and pressure overload in rats. (A)** Summary of qualified CM nuclear transcriptomes in NF hearts in O vs Y rats and in AB vs Sham rats. **(B)** UMAP of the CM nuclear transcriptomes from the Y vs O. and Sham vs AB (L: Loose_AB, T: Tight_AB) and distribution of the two CM subpopulations across the conditions. **(C)** Proportion of the CM nuclei subpopulations in the Y vs O and HF vs Sham (S). **(D)** DEGs identified in the CM nuclei subpopulations. **(E)** Top enriched pathways associated with the CM subpopulations DEGs. **(F)** RT-qPCR analysis of the expression of stress and hypertrophy-associated marker genes in RNA isolated from CM nuclei purified from the LV Y vs. O (top), and in Sham (S) with Loose (L) and Tight (T) AB animals (bottom). **(G)** Heterogeneity of CM nuclear transcriptomes between Y and O samples and the AB versus Sham (p-value was calculated based on the Wilcoxon test). **(H)** Top: Trajectory of transcriptomic alterations across nuclei. Y vs O and Sham vs AB are shown. Frequency of nuclei pseudotimes in the Y vs O and Sham vs AB.

## Rat CM phenotypic remodeling induced by aging and pressure overload

We next probed for conservation of findings in human CM with CM from rodent aging and models of cardiac pathology. Aging was studied in Y (3 months) and O (26 months) Sprague Dawley rats (Fig. 6A; Table 5). Hypertrophic remodeling of the heart and HF were induced by mild or severe pressure overload subsequent to a mild or severe constriction of the ascending aorta (aortic banding; AB) using silicon bands (mild stenosis (Loose, L: 1.5 mm) or severe stenosis (tight, T: 1.07 mm)) that was imposed on 6-week-old animals and allowed to develop over 6 weeks [25]. Sham-operated animals (S) were included as controls (Fig. 6E; Table 6).

Animals were deeply phenotyped (Supplementary 15; Tables 5, 6). Relative to Y, O rats exhibited impaired diastolic function (decreased e', increased E/e' and E/A) and systolic function, evidenced by decreased fractional shortening (FS; Fig. 6B; Table 5). O rats exhibited no impairment in global longitudinal strain (GLS) but showed impaired global circumferential strain (GCS) (Table 5). Systolic and diastolic circumferential and longitudinal strain rates were both impaired in O vs Y. While HW (heart weight), LVW (left ventricle weight) and LVIDs (Left ventricular internal diameter in systole) were increased significantly, IVSd (Interventricular septal thickness at end-diastole), IVSs (Interventricular septal thickness at end-systole), and LVIDd (Left ventricular internal diameter in diastole) were unaffected (Table 5). Consistent with development of deleterious remodelling, LW (lung weight) and LAD (Left atrial diameter) were also increased in aging (Fig. 6B; Table 5). Masson trichrome staining revealed (Fig. 6C) increased collagen deposition between Y and O rat hearts, which was also reflected by increases in Periostin (*Postn*), a marker of activated FB. *Col1a2* and *Col3a1* were however unchanged (Supplementary Fig. 15A). Expression of the MCP-1 (*Ccl2),* a marker of inflammation was also increased (Supplementary Fig. 15A). Indicative of CM stress and hypertrophy, tissue level expression of *Nppa*, *Nppb*, *Myh7*, *Acta1* and *Xirp2* were increased between Y and O, whereas *Myh6* was decreased (Fig. 6D; Supplementary Fig. 15A). *Atp2a2*, encoding SERCA2a and *Ryr2,* involved in $Ca^{2+}$ clearance and release in CM were unchanged and decreased respectively between Y and O (Supplementary Fig. 15A). No difference in expression of senescence associated β-galactosidase (*Glb1*) was detected (Supplementary Fig. 15A).

AB-induced remodeling was related to the severity of the stenosis applied (Fig. 6E), which was confirmed by the pressure gradient across the stenosis (Table 6). AB animals exhibited reduced systolic function (FS) but no change in diastolic function (E/A and E/e') (Fig. 6F; Table 6). While GLS (not GCS) was reduced in response to mild stenosis, a dramatic reduction in both measures was detected in severe stenosis (Table 6). Systolic circumferential and longitudinal strain rates were both reduced in response to mild and severe stenosis while diastolic longitudinal strain was only reduced in severe stenosis. Mild stenosis induced a significant hypertrophic response as shown by cardiac/LV mass measurements ($LVW/TL^3$) and echocardiography (increases in septal and posterior wall thickness; IVSd and LVPWd) but did not develop HF (Table 6). No changes in LV internal diameter in diastole or systole or in FS were detected in these animals (Fig. 6F; Table 6). Moreover, LAD and LW were also no different from Sham rats (Fig. 6F; Table 6), indicating a compensatory hypertrophic response without failure. Consistent with HF, severe stenosis resulted in decreased FS (Fig. 6F), increased LW, indicative of pulmonary congestion and LAD (Fig. 6F; Table 6). These rats further showed substantial remodeling in myocardial thickness (IVSd and LVPWd) and chamber dimensions (increases in LVIDd and LVIDs), indicating a dilation of the LV (Table 6).

Histological analysis showed increased fibrosis in AB with a significant increase in interstitial collagen detected ($p=0.0076$) (Fig. 6G). RT-qPCR analysis of RNA isolated from tissue showed significant increases in *Nppa* and *Acta1* in mild and severe stenosis and but no change in *Nppb* (Fig. 6H; Supplementary Fig. 15B). *Myh6* and *Myh7* were only decreased and increased respectively following severe stenosis (Fig. 6H). *Xirp2* was also only significantly increased with severe stenosis. Fibrotic (*Postn, Col3a1)* and inflammatory markers (*Ccl2)* (Supplementary Fig. 15B) were increased in banded animals, although *Postn* was upregulated only in response to severe stenosis. *Col1a2* was also significantly increased in the tight banded group. Consistent with previous

reports and diminished $Ca^{2+}$ handling in HF, *Atp2a2*, encoding SERCA2a and *Ryr2* (RyR2) involved in $Ca^{2+}$ clearance and release in CM were reduced in severe stenosis (Supplementary Fig. 15B). In contrast to aging, expression of senescence associated β-galactosidase (*Glb1*) was increased in response to both mild and severe stenosis (Supplementary Fig. 15A).

Together, these, functional, molecular and histological analysis identify differences in cardiac remodeling between aging and pathology. While during both aging and in response to mild stenosis, a mild hypertrophic response is observed, a greater hypertrophic response associated with reduced function is induced by the more severe stenosis.

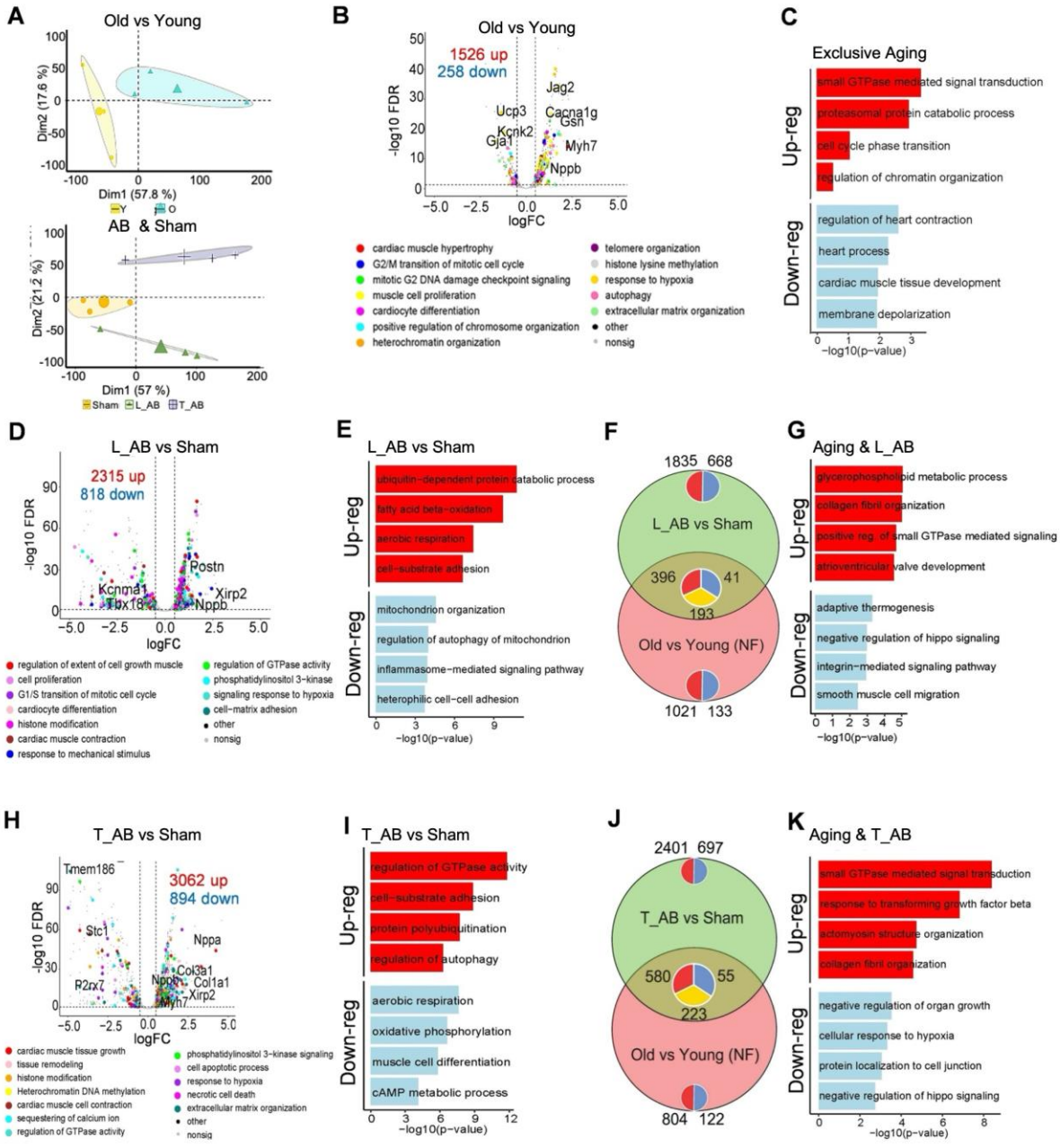


**Figure 8. Comparison of transcriptome remodeling during aging and in response to pressure overload in rats by pseudobulk analysis. (A)** PCA plots of Y vs O (top) and Sham vs AB (bottom) samples. **(B)** DEGs identified in the comparison of CM nuclei from O vs Y samples. **(C)** Enriched pathways amongst the exclusive DEGs in Y vs O. **(D)** DEGs in loose-AB versus Sham. **(E)** Top enriched pathways of the exclusive DEGs in loose-AB vs Sham. **(F)** Shared and distinct DEGs in Y vs O (NF) and loose-AB versus Sham. **(G)** Top enriched pathways of the shared DEGs in loose-AB vs Sham and Y vs O. **(H)**

DEGs in tight-AB vs Sham. I) Top enriched pathways of the exclusive DEGs in tight-AB vs Sham. **(J)** Shared and distinct DEGs in Y vs O and tight-AB vs Sham. **(K)** Top enriched pathways of the shared DEGs in Tight-AB vs Sham and Y vs O. In the Venn diagrams, red and blue indicate consistently up- or downregulated DEGs; yellow indicates shared DEGs with opposing regulation between comparisons.

**Aging and pressure overload induce distinct alterations in rat CM transcriptomes**

To uncover CM specific transcriptomic changes and how they impact CM states, we performed snRNA-Seq (VASA-Seq) on FACS-purified PCM-1/PLN labelled CM nuclei. This analysis yielded 1380 qualified single-nuclear transcriptomes across the groups (Fig. 7A) (mean 55906 uniquely mapped reads and 9347 genes detected). Transcriptomes from Y vs O and Sham vs AB were integrated using Harmony. They were then visualized on their own UMAPs (Fig. 7B) revealing 2 distinct CMs subpopulations (CM1 and CM2) (Fig. 7C). CM2 was predominant in Y and S and was almost completely replaced by CM1 with age, whereas with AB (mild and severe stenosis), the shifts to CM1 were similar and not so dramatic (Fig. 7C). CM1 expressed stress-related genes associated with pathological hypertrophic remodeling and the so-called foetal gene programme, including *Myh7* and *Acta1* and low expression of *Myh6*, whereas CM2 expressed high *Myh6* and low *Myh7* (Fig. 7D; Supplementary File 20). CM1 was enriched for processes related to cardiac muscle cell repolarization and inositol phosphate biosynthetic processes while CM2 was enriched for processes associated with cardiac muscle cell morphogenesis and voltage-gated sodium channel activity (Fig. 7E). Consistent with the CM remodeling detected in the snRNA-Seq, RT-qPCR analysis on mRNA isolated from purified CM nuclei (Fig. 7F) showed increased expression of *Nppa* and *Myh7* in O versus Y, and increased *Nppa* and *Nppb* and decreased *Myh6* in severe stenosis. While *Nppa* and *Nppb* were also induced in mild stenosis, *Myh6* was unchanged (Fig. 7F).

**CM heterogeneity is increased in rat aging and in response to pressure overload.**

As a measure of CM heterogeneity, we next determined Euclidean distances between CM nuclear transcriptomes. Heterogeneity significantly increased with both age and pressure overload, which was greater in the severe than mild stenosis groups (Fig. 7G). Top variable genes with aging included *Ptgfr* (receptor for prostaglandin F2-alpha, a lipid mediator [78]), *Ypel2* (associated with cell cycle regulation, mitosis, and senescence [79]), *Ppargc1a* (a master regulator of mitochondrial biogenesis and energy metabolism [80]), and *Abhd2* (linked to lipid signaling [81]) (Supplementary File 21). Top variable genes in mild stenosis included *Fnip2* (involved in cellular metabolism and energy regulation [82]), *Gpm6a* (associated with stress responses [83]), *Ugp2* (involved in energy storage, cell metabolism [84]), *Ppargc1a*, and *Pik3r1* (involved in cell growth, metabolism, and survival [85]) (Supplementary File 21), and in the severe stenosis group, *Gda* (involved in nucleotide turnover and nitrogen excretion [86]), *Nuak1* (associated with energy metabolism, cell survival, and stress response [87]), *Pkhd1l1* (linked to cell movement [88]), *Serpine1* (involved in ECM remodelling, and cell migration [89]), and *Per3* (involved in circadian rhythms [90]) (Supplementary File 21). Notably, consistent with the evolution of remodelling, trajectory analysis indicated that the pseudo-times progressed from Y to O and from Sham to AB (Fig. 7H).

**Overlap of DEG between age and pressure overload is greatest in severe stenosis**

DEG associated with age and pressure overload in rat CM were identified through a pseudo-bulk analysis. Transcriptomes of each group were distinctly distributed in the PCA plot (Fig. 8A). Between O and Y, 1526 genes were significantly upregulated and 258 downregulated (Fig. 8B; Supplementary File 22). DEG were associated with cardiac hypertrophy, G2/M transition, and histone modifications. Among these genes, 591 upregulated and 70 downregulated genes were unique to aging (Supplementary File 22). Exclusively upregulated genes were linked to small GTPase-mediated signal transduction, cell cycle phase transitions, and chromatin organization. Exclusively downregulated genes were associated with heart contraction regulation, muscle tissue development, and membrane potential regulation (Fig. 8C). In response to mild stenosis, 2315 upregulated and 818 downregulated genes were detected (Fig. 8D; Supplementary File 23), which were associated with regulation of muscle growth, G1 to S transition, and histone modifications (Fig. 8D). Upregulated DEGs exclusive to mild stenosis versus Sham were linked to catabolic protein process, fatty acid beta-oxidation, cell-substrate adhesion, while downregulated genes were involved in mitochondrial organization, mitophagy, inflammation pathways, and cell-cell adhesion (Fig. 8E; Supplementary File 23). Out of these DEG, 396 and 41 genes overlapped with genes also up- and down-regulated respectively with aging (Fig. 8F). The shared upregulated genes were involved in glycerophospholipid metabolism, collagen fibril organization, small GTPase signaling, and

atrioventricular valve development (Fig. 8G; Supplementary File 23). Shared downregulated genes were associated with adaptive thermogenesis, hippo signaling, smooth muscle cell migration and integrin mediated signaling pathway (Fig. 8G; Supplementary File 23). In severe stenosis, 3062 genes were up- and 894 down-regulated (Fig. 8H; Supplementary File 24). DEG were involved in muscle tissue growth, tissue remodelling, DNA methylation, calcium ion transport, and necrotic cell death. Genes uniquely upregulated with severe stenosis were associated with protein catabolic processes, autophagy, cell substrate adhesion, and GTPase activity, while genes exclusively downregulated were involved in muscle cell differentiation, aerobic respiration, oxidative phosphorylation, and cAMP metabolic process (Fig. 8I, Supplementary File 24). Importantly, while DEG were condition specific, many of the pathways they populated were shared between age and pressure overload. Amongst the DEG in severe stenosis, 580 upregulated and 55 downregulated genes were also observed during aging (Fig. 8J). The shared upregulated genes contributed to processes underlying fibrosis, including TGF-β signaling, small GTPase-mediated signal transduction, actomyosin structure organization, and collagen fibril organization (Fig. 8K; Supplementary File 24). Shared downregulated genes were linked to the negative regulation of organ growth, response to hypoxia, cell junction assembly, and hippo signaling (Fig. 8K; Supplementary File 24).

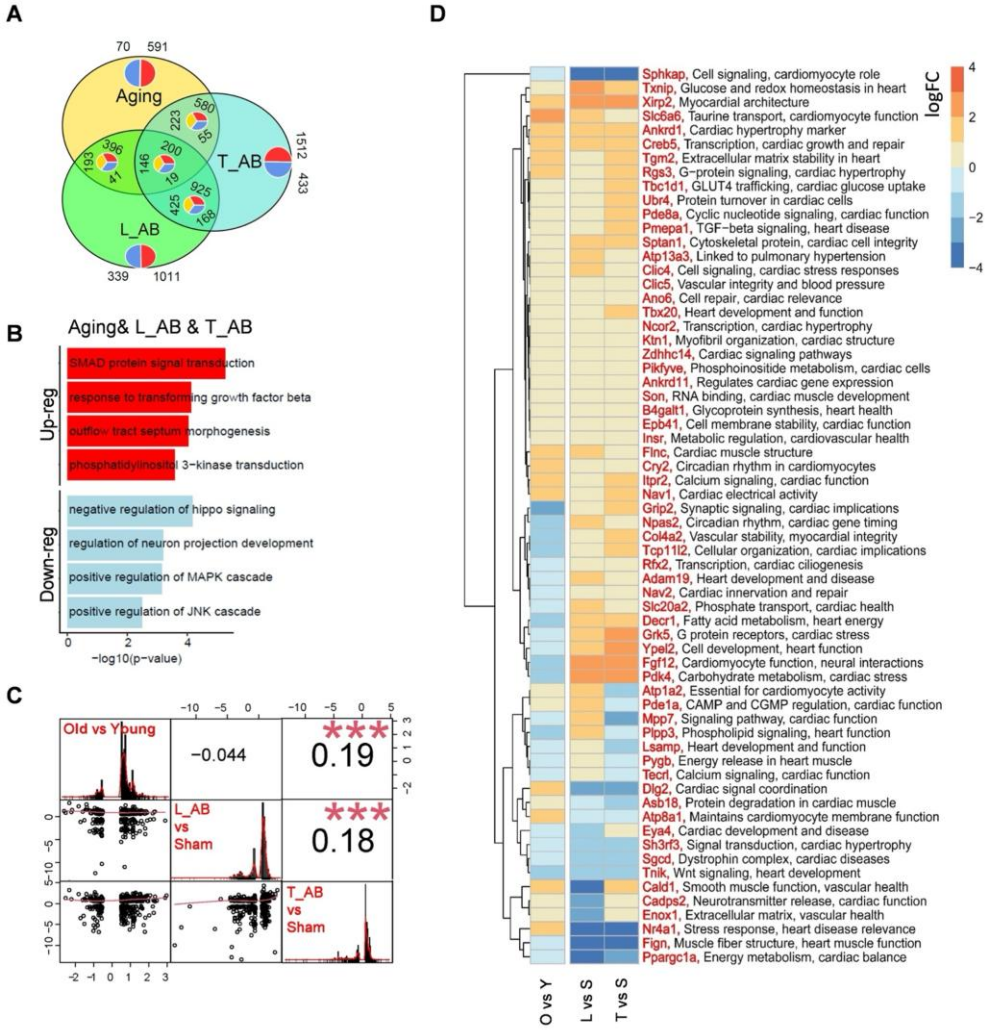


**Figure 9. Correlation analysis of transcriptome remodeling in aging and in response to pressure overload in rats. (A)** DEGs shared between aging and AB and **(B)** their associated pathways. **(C)** Spearman's Rank-Order correlation based on the total of the detected DEGs in the comparisons. **(D)** Heatmap of the DEGs shared between aging and AB (aggregated gene expression values > 100, taken from every nucleus within each sample). In the Venn diagram, red and blue indicate consistently up- or downregulated DEGs; yellow marks shared DEGs with opposing regulation between comparisons.

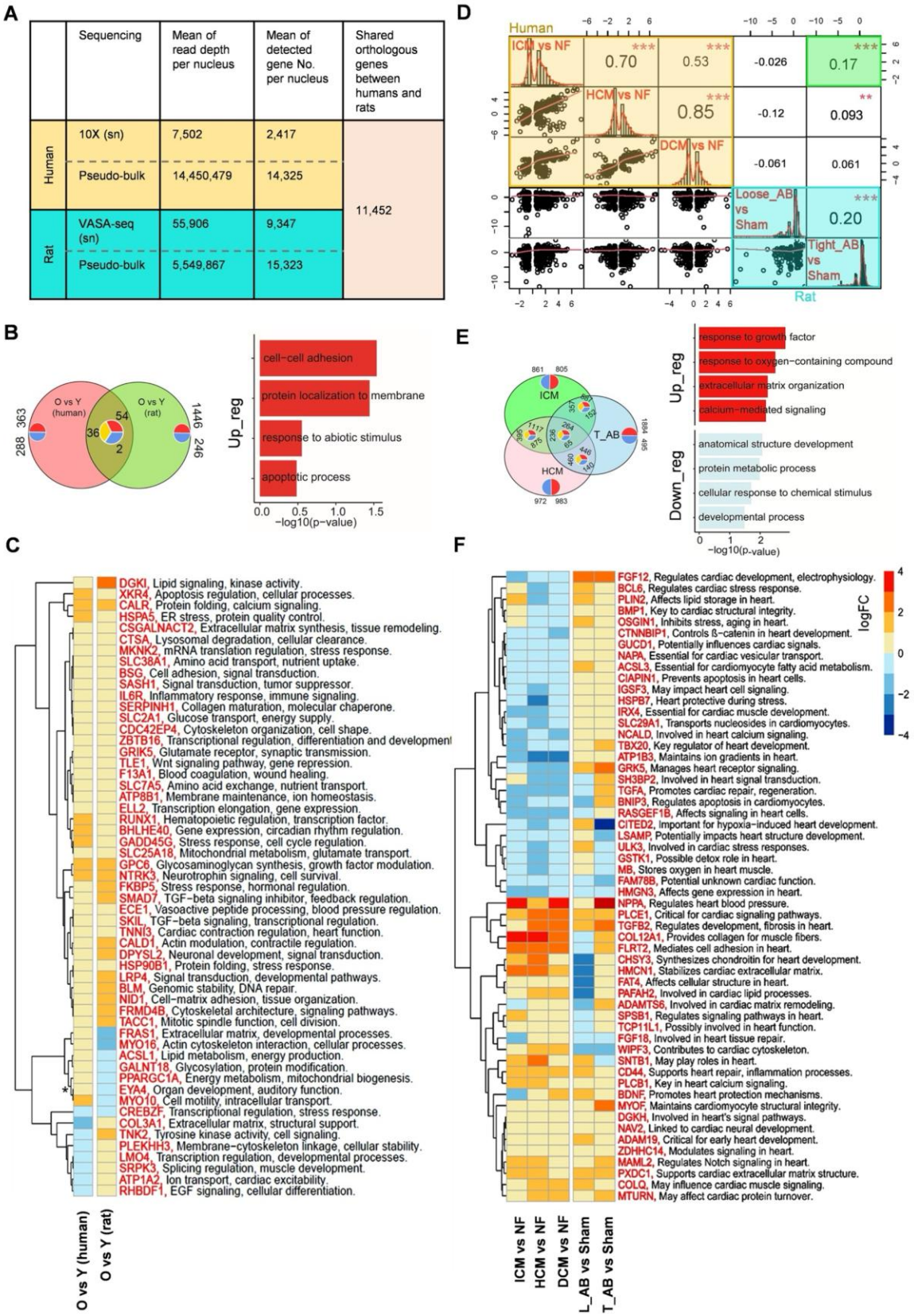


**Figure 10. Comparison between transcriptome remodeling in response to pathology and aging in human and rat.** **(A)** Mean library read depth and mean number of detected genes in snRNA-Seq data from humans and rats, along with the

orthologous genes shared between the two species. **(B)** Shared and unique DEGs between human and rat aging and enriched pathways associated with the shared upregulated genes. **(C)** Heatmaps of shared DEGs between humans and rats aging **(D)** Correlation between human and rat pathology based on the shared DEGs in all the comparisons. **(E)** Shared and distinct DEGs between human and rat pathologies and enriched pathways associated with shared DEGs (ICM, HCM and T_AB as the most correlated conditions were included). **(F)** Heatmaps of the shared DEGs between human and rat pathological conditions. In C and F, only genes with aggregated gene expression values >100, taken from every nucleus within each sample were included. In the Venn diagram, red and blue indicate consistently up- or downregulated DEGs; yellow marks shared DEGs with opposing regulation between comparisons.

Intersection of DEG from all condition comparisons to identify hallmarks of cardiac remodelling, identified 200 up- and 19 down-regulated genes (Fig. 9A; Supplementary File 25). Upregulated genes were associated with SMAD signaling (*Bmp6* and *Smad6*), response to TGF-β (e.g. *Ankrd1, Col3a1, Tgfb2*), outflow tract septum morphogenesis (e.g. *Nrp2, Tbx20*), regulation of phosphatidylinositol 3-kinase/protein kinase B signal transduction (e.g. *Insr* and *Pdgfrb*), while downregulated genes were associated with MAPK, JNK, hippo signaling as well as neuron projection during development (Fig. 9 B; Supplementary File 25). The correlation between DEGs in the severe stenosis group showed a stronger, albeit weak correlation (r= 0.19), with aging than in the mild stenosis group (Fig. 9C). Prominent DEG unique to or shared between aging and AB (mild and severe) are presented in Fig. 9D. These include the established markers of CM stress *Xirp2*, *Ankrd1*, and *Itpr2*, which are upregulated in aging and pressure overload, while *Nr4a1* and *Atp8a1* were uniquely upregulated in aging (Fig. 9D). Changes in expression of genes involved in CM electrophysiology (action potential generation and calcium handling) and in glycolysis clearly illustrate functional remodeling of CM in age and disease and the distinct response to aging and to mild and severe stenosis (Supplementary Fig. 16).

We further examined whether *Prelid2* and *Grxcr2*, downregulated in pathology and upregulated in age in human and enriched in CM were differentially expressed in rat LV samples under these conditions. RT-qPCR analysis determined that *Prelid2* was increased in aging rat but unchanged in AB while *Grxcr2* did not change in age or pathology (Supplementary Fig. 15C).

To gain insight into upstream regulatory mechanisms underlying the transcriptional alterations detected, we performed transcription factor (TF) motif analysis on the 500 bp upstream and 100 bp downstream of the TSS of identified DEGs (Table 7). This analysis identified the motif for *Taf1* as being commonly enriched on upregulated DEGs in both aging (35 genes) and in response to AB (823 genes in mild stenosis and 969 in severe stenosis vs Sham, Supplementary File 26). Interestingly, *Taf,* which together with the TATA-binding protein (TBP) forms the basal transcription factor TFIID, was also upregulated in both aging and AB vs Sham (Supplementary Fig. 17).

**Shared and unique pathways between human and rat in response to age and pathology**

We next investigated whether any DEG, gene ontologies and pathways identified in disease and aging in our analysis of rat and human were shared between species. Integration of human and rat pseudo-bulk gene expression matrices identified 11452 orthologues genes (Fig. 10A). Between rat and human aging, 54 upregulated and 2 downregulated genes were shared. 36 genes showing opposing changes between species (Fig. 10B; Supplementary File 27). Shared upregulated DEGs were associated with cell-cell adhesion (*NRXN2*, *LRRC4B*, *ENTPD1*, *RUNX1*, *CDH22*), protein localization to membrance (*NRXN2*, *HSPA5*, *GPC6*), response to abiotic stimulus (*NRXN2*, *CALR*, *BHLHE40*, *BLM*, *SLC7A5*, *HSP90B1*), and apoptotic process (*XKR4*, *CALR*, *HSPA5*). mRNAs encoding the CREBZF1 transcription factor and the Regulator Of Telomere Elongation Helicase 1 (*RTEL1*), which stabilizes telomeres, were downregulated in both species. Shared DEGs between human and rat aging, with a summed expression greater than 100 per sample, are shown in Fig. 10C.

Across human CMPs and pressure overload severity in rats, 2,292 DEGs were identified with the greatest correlation found between rat severe stenosis and ICM (r=0.17, Fig. 10D; Supplementary File 27). 264 upregulated and 65 downregulated genes were shared between ICM and HCM in humans and severe stenosis in rat (Fig. 10E; Supplementary File 27), which were associated with 'response to oxygen-containing compound' (e.g. *ACE* and *SESN3*), 'calcium-mediated signaling' (e.g. *PLCG2*, and *CMKLR1*), 'ECM organization' (e.g. *COL3A1*, *COL5A1*, *COL5A2*). Prominent shared DEGs, exhibiting either similar or contrasting expression patterns between humans and rats in pathology, are displayed in the heatmap (Fig. 10F).

Given that many genes appearing in aging and pathology in rat and human belonged to similar functional classes with established roles in cardiac remodelling, we also compared the overlap between up- and down-regulated GO across our human and rat datasets (Supplementary Fig. 18; Supplementary File 27). Across disease in human and rat, other than in human DCM, the GOs with the greatest number of altered genes included calcium handling, ECM, transcription factors, cellular

respiration and apoptosis. Notably, consistent with the metabolic phenotype of HCM, cellular respiration was the most altered GO in this disease. ECM was, however, most differentially affected in ICM in human and was one of the most affected in severe stenosis in rats. Notably, while cellular respiration was as in human also altered in rat, this GO was most enriched in the milder stenosis than following severe stenosis where rats were in HF.

## DISCUSSION

Here we define how CM states, heterogeneity, and regulatory programs shift with age and how these changes overlap with, but are not identical to, those observed in CMPs. These findings were achieved by integration and analysis of human snRNA-Seq datasets covering different CMP and age, and their comparison with snRNA-Seq data from deeply phenotyped rat models of aging and pressure overload, In rats, we show that physiologic aging and hypertrophy and HF induced by aortic banding share key features with human, with mild pressure overload resembling aging and severe stenosis aligning with ICM-like signatures. Validating our analysis, this cross-species orthology identified calcium signaling, ECM organization, and stress responses, well-established processes dysregulated in age and pathology, that were shared between rat and human (Supplementary Fig. 18).

### CM states are differentially remodelled in human aging and pathology

Single-nucleus/cell approaches have provided new insights into the diversity of cell types and states in the heart and how they change with disease. Through these means, cell-type specific mechanisms underlying the complex structural remodeling of the heart involving fibrosis and CM hypertrophy can be obtained. Indeed, consistent with CM death and associated fibrotic remodeling described in disease and aging, a decrease in the proportion of CM with aging and during ICM and HCM was detected. Notably, while the proportion of FB were increased in disease, this was not the case in aging. This lack of an increase in FB proportion with aging may represent the more chronic fibrotic remodeling of the aged human heart where existing fibrosis and ECM remodeling no longer involves substantial persistent activation and proliferation of FBs.

As well as altering in relative abundance, CM nuclei were redistributed among established CM substates in pathology but not in aging [20]. In CMP, the more basal vCM1 [20] was most abundant in all groups, and, while changes in its proportion between conditions were detected, these were not great in magnitude. Most significant changes were observed in vCM2, 3 and 4. Of these prevalent cell states, vCM2 was markedly decreased and vCM3 increased in ICM, HCM, and DCM. The decrease in vCM2, a state enriched for contraction/action-potential genes and very similar to the basal vCM1 but also expressing *PRELID2*, linked to mitochondrial phospholipid metabolism [91], and increase in vCM3 enriched for stress-responsive genes (*ANKRD1*, *FHL1*, *XIRP2)* linked to CMP are consistent with adverse remodeling of CM [92]. The minor cell type vCM4 was significantly diminished in HCM. This cell state shows elevated levels of CRYAB (a cytoprotective heat shock protein) [63], as well as genes encoding sarcomeric proteins and ion channel associated with arrhythmias (e.g. *FHL2*, *FHL1*, *ANKRD1*, *NEXN* and *PLN*). The expression of these stress, and cytoprotective genes in vCM3 and 4 is suggestive of these cells being exposed to stress or that these populations represent a more immature phenotype. vCM5 constitutes approximately 1% of all ventricular CMs and is implicated in compensatory mechanisms during CM loss in ICM, possibly influencing electrophysiology due to its notable expression of the EBF1 transcription factor [93]. This TF is of potential relevance owing to its association with myocardial hypercellularity, reduced CM size, ventricular conduction system hypoplasia, and conduction system disease in Ebf1-deficient hearts [94].

### Cellular and transcriptional heterogeneity is increased in aging and in cardiomyopathy

Through contributing to loss of cell identity and/or transcriptional misregulation, increased cellular and transcriptional heterogeneity is increasingly recognised as a contributor to age and pathology. However, while an age-associated increase in cell heterogeneity is established in cells from other tissues in human, e.g. in skeletal muscle, studies in CM are limited [12, 95]. Greater heterogeneity in CM with aging is however reported albeit in 33663 cells where ~10,000 transcripts were analysed [18]. By analysing the extensive dataset of CM transcriptomes available to us, we could robustly establish greater cellular heterogeneity, as well as of individual transcripts during aging and in CMPs. These findings in aging and diseased human CM add to our analysis of post-MI remodeling in pig, where we identified increased transcriptomic diversity as a contributor to electrophysiological heterogeneity within CM populations in the infarct border zone [21]. Indeed, here in human aging, as previously in the MI border zone in pig, the greater heterogeneity between cells was associated with increased numbers of CM expressing stress/hypertrophy-related genes, such as *NPPB* and *XIRP2* - cell states more prevalent in disease. This finding may allude to the heterogeneity in cell phenotypes that

arise through aging in NF CM, including via degradation of the epigenome and loss of silencing of genes enriched in earlier life stages [11]. This increased cell to cell variance in expression of *PLCG2*, *NPPB*, and *MYL7* in aging CMs may have significant implications for contractile dysfunction, the development of arrhythmias, and heterogeneous hypertrophic remodeling [96-98]. Supporting this notion, mosaicism in mice harbouring HCM mutations results in heterogeneous cellular behaviours leading to reduced contraction [99], and increased CM heterogeneity in the MI border zone in pig is associated with heterogeneity in action potential profiles and greater arrhythmogenicity [21].

**DEGs, their regulating TFs and associated pathways in aging and cardiomyopathy**

By DEG and trajectory pseudotime analysis, overlapping and distinct features of CM remodeling during age and pathology were identified. Notably, while certain of these DEG were lost in a leave one out sensitivity analysis, the majority were retained, particularly for upregulated DEG. Lost genes were primarily those that showed a lower fold change or FDR supporting the notion that our strategy to increase sample and cell numbers through integrating datasets to increase statistical power of analysis is a robust strategy to identify disease- and aging-related DEG and pathways. However, while inclusion of datasets that describe sample types that are not equally distributed across all datasets (e.g. HCM in our analysis, which was present only in a single study [17]) have utility for identification of genes and pathways that they share or not with other sample types (DCM and ICM in our analysis), they may disproportionally impact the overall dataset. DEGs associated with aging and CMP reflect those reported in other studies of cardiac remodeling and include pathways linked to cardiac hypertrophy, calcium transport, histone modifications, cell cycle regulation, potassium transport, oxidative metabolism and ECM organization [17-20]. Correlation analysis revealed stronger similarity between aging and HCM suggesting that "physiologic" age associated remodeling partially phenocopies the hypertrophic adaptation, consistent with preserved systolic function and impaired relaxation often seen with aging [5]. In contrast, ICM and DCM additionally engaged immune/fibrotic (ICM) and vascular/TGF-β (DCM) axes and displayed greater repression of respiratory and contractile machinery as well as deleterious remodeling of ion channel and calcium handling genes. While DEG analysis was based on pooled CM nuclei for each condition, trajectory analysis could show the evolution of the remodeling process and how during earlier stages, significant overlap between the trajectories of transcriptional remodeling of CM nuclei during aging and from NF to CMPs was detected. At later stages of remodelling, we detected a divergence into condition-specific branches. Highly expressed genes along the trajectory branch exclusive to aging were involved in cardiac tissue morphogenesis and organelle organization. Conversely, transcriptome changes in the region of the trajectory shared between aging and CMP reflected processes related to muscle adaptation and cell adhesion (e.g., *MYH7* [100], *VCL* [101], *CTNND2* [102]), which potentially contribute to cardiac dysfunction, fibrosis, and contractile abnormalities. The increased frequency of nuclei assigned to later trajectories in older individuals than those with CMP suggests that with aging of NF CM, more CM have reached their terminal aged stage whereas in CMP, remodeling is ongoing.

Aging- and CMP-related DEGs exhibit distinct TF motifs in their regulatory regions. While many shared DEGs and trajectories were identified between aging and pathological conditions, no regulatory TF motifs (motif present and TF upregulated) were found to be shared between these conditions. This finding would suggest that, at the level of transcriptional regulation, mechanisms for disease induction differ between age and the various pathologies and likely reflect the differences in the initiating cues involved. Indeed, age may involve a progressive integration of various age-related stressors, including pressure overload, ischemia and inflammation acting on a background of a deregulating epigenome to allow expression of pathology-related genes [103]. In pathology on the other hand, disease is manifest in younger individuals and is induced by more acute stressors. TF motifs specific to age or CMP were however identified. Notably, age-related DEG are enriched for a recognition motif for HMGA2, a chromatin-modifying gene that cooperates with the repressive chromatin mark H3K9me3 and heterochromatin protein 1 (HP1α), involved in formation and stabilization of heterochromatin. Moreover, and supporting a functional role, HMGA2 expression was also increased. The potential importance of HMGA2 in aging is supported by its recent identification in a GWAS study of cardiac age acceleration [104]. In aging HMGA2 is involved in senescence and inflammation, where it is involved in the formation of senescence-associated heterochromatin foci (SAHF) [105]. HMGA2-associated regulatory activity has been linked to expression of the cell cycle inhibitor CDKN2C (p18INK4c)(Fig. 5A, Supplementary File 19), which can induce cell cycle arrest, induction of IL6R expression, which is upregulated in aging, and with the senescence-associated secretory phenotype (SASP) that contributes to age-related inflammation and tissue remodeling [106]. Further, HMGA2 motifs were identified in DEG linked to cellular stress response and apoptosis regulation in NF aging (Supplementary File 18

and 19) [107-109]. HMGA2 target genes involved in lipid metabolism and energy homeostasis [110, 111], were also upregulated, suggesting an involvement of HMGA2-associated transcriptional programs in metabolic remodeling in aged CM. Indeed, while not altered in ICM vs NF, HMGA2 together with genes involved in metabolism were coordinately differentially expressed between Y and O ICM CM, supporting a role in disease progression in the aging ICM context. Upregulated HMGA2 target genes also include those associated with ECM in aging that contribute to fibrosis and tissue stiffening that are well described features of aging-associated cardiac dysfunction [112]. Consistent with this, our analysis of the interaction between age and ICM revealed that aging was accompanied by marked metabolic remodelling, downregulation of chromatin regulators, and widespread repression of structural and calcium-handling genes. Only a small subset of these DEGs overlapped with aging in NF CM, supporting the notion that in this older ICM group, the presence of pathology dominates over aging-related changes. Shared upregulated genes such as *HMGA2*, *ORAI2*, and *NRG1* may represent general markers or components of aging-associated cardiac remodelling, whereas ICM-specific alterations in regulators like *IGF1R*, *SMAD7*, and *MMP2* likely contribute to pathological progression.

Potentially reflecting convergence of cellular phenotype between CMP of different etiologies, shared regulatory TF motifs were identified amongst DEG associated with ICM, HCM, and DCM [113]. Upregulated TFs, including *BCL6B, ELK3, ERG*, and *FLI1*, showed enriched motifs in genes upregulated in both ICM and HCM. *Bcl6b* and *Elk3*, along with *Fli1*, *Sox18*, and *Lyl1* have previously been identified as regulators of angioblast-specific gene expression during embryo-genesis in mice, suggesting an important role in mesodermal lineage development [114]. Interestingly, the motif for ATF3 emerged as a TF motif enriched among the downregulated genes in HCM and DCM. ATF3 plays an essential role in maintaining CM homeostasis and coordinating systemic glucose metabolism [115]; its reduced expression in HCM and DCM may contribute to the metabolic alterations in disease leading to pathological remodelling.

**Co-expression analysis identifies candidate genes associated with aging and cardiomyopathies**

WGCNA analysis identified candidate hub co-expressed genes associated with the aging process and their overlap with pathological conditions. These genes can be functionally categorized into major biological processes relevant to aging and cardiovascular dysfunction. Of note, 'Mitochondrial Function' and 'Oxidative Stress', central players in cardiac aging were perturbed. Apart from the expected decreased expression of genes involved in mitochondrial respiration, *METTL17*, which has been linked to mitochondrial RNA methylation, mitochondrial protein synthesis, energy production, and oxidative stress [69], was downregulated in both aging and HCM. Consistently present in the analysis and again in the WGCNA were alterations in 'Calcium Signaling' and 'Contractile Dysfunction'. In this WGCNA analysis, ORAI2, a component of store-operated plasma membrane calcium channels, previously implicated in CM hypertrophic signaling [116], was upregulated. At the level of gene expression regulation, 'Chromatin Remodelling', 'Cell Cycle Regulation', and 'Transcriptional Regulation' were also present. The upregulation of *JADE1* and *CDKN2C* is consistent with alterations in chromatin remodeling [117] and cell cycle regulation [118], respectively, influencing cellular senescence and other aging-related processes. The downregulation of *PHF1*, a histone-binding protein promoting H3K27 methylation [119], along with lower levels of *EHMT2*, an H3K9 dimethyltransferase [11], suggests disruption of chromatin structure and transcriptional regulation. Indeed, HDACs were particularly prevalent amongst downregulated genes (Supplementary File 9, 10, and 11) in aging ICM vs NF (*HDAC7*, *HDAC10*), HCM vs NF (*HDAC5, 6, 9*) and DCM vs NF (*HDAC9*). Together with the reduction in HMGA2 in aging in CM from NF hearts, an additional reduced expression of HDACs in ICM aging may contribute to altered transcriptional states that accompany myocardial remodeling in aging ICM.

**DEG in aging and cardiomyopathy overlap with CVD risk loci identified by GWAS**

Our integrative analysis identified an intersection of age-associated DEG with inherited genetic risk loci for CVD. By overlaying aging DEGs with GWAS-eQTL datasets from non-congenital CVD, we identified loci including *FUT11*, *FCHO1*, and *NMB*, where the direction of age-related expression change aligned with the effect of risk alleles on gene expression. Similarly, in ICM, several established loci (*APOB*, *CYP21A2*, *EXOSC5*, *RNF215*, *TBX20*, *TCF21*) showed concordant overlap between patient-derived DEGs and GWAS-eQTL signals. These results suggest that transcriptional changes arising during cardiac aging partially recapitulate genetic mechanisms that predispose to disease. However, eQTLs were derived from bulk left ventricular tissue (GTEx), which captures the impact of a SNP on gene expression arising from the diverse cell types of the heart, whereas our expression data was derived from CM alone, which represent fewer than 25% of cardiac cells. Since GWAS loci for CVD

involve processes mediated by endothelial, fibroblast, immune, or vascular smooth muscle cells [120, 121], some overlaps we observed may reflect effects reported in non-CM populations, even though only CM DEGs were tested here. The subjective grouping of SNPs into CVD-related traits may further obscure the relationship between gene expression changes in CM and CVD related SNPs. Further, the requirement for genome-wide significance (GWAS $p < 5 \times 10^{-8}$) and stringent eQTL thresholds reduces false positives but may also exclude moderate, biologically relevant signals. In addition, while we define "true concordance" when eQTL and DEG directions match, such agreement does not prove causality; pleiotropic effects or age-dependent reprogramming could produce similar signatures. Another consideration is that SNP-to-gene assignments remain uncertain, as many GWAS variants regulate multiple or distal genes [122]. Despite these limitations, our findings highlight the value of integrating human genetic data with snRNA-Seq data to prioritize candidate genes for mechanistic study. Genes such as *FUT11* and *FCHO1*, which are upregulated with age and further increased by risk alleles, emerge as potential mediators of maladaptive remodeling in the aging ventricle. Future studies leveraging single-cell or condition-specific eQTL maps [123] and formal GWAS-eQTL colocalization will be essential to confirm causal mechanisms. Taken together, our results suggest that a subset of age-driven transcriptional changes in CM mirrors genetic susceptibility to CVD, providing an entry point for investigation of and distinguishing how age and inherited risk converge to affect human cardiac pathology.

**Transcriptomic remodeling of rat CM during pathology and age shares features with human**

In rats as in human, our data reveal distinct features of CM in aging and pathology. Our rat models provide more controlled forms of cardiac and CM remodeling associated with aging (in the absence of comorbidities) and with compensated and decompensated hypertrophy/HF that allowed stronger relationships between DEG and phenotypic changes under these conditions to be established. Indeed, gross measures of remodeling in rat during age and under conditions of mild and severe pressure overload reflected those in human in age and hypertrophic and ischemic pathology respectively. Mild stenosis induced concentric cardiac hypertrophy without failure and an altered transcriptome that shared several hundred DEGs with aging, whereas severe stenosis led to HF, chamber dilation, increased left atrial dimensions, pulmonary congestion, and a transcriptome that reflected ICM HF in human. Aged rat hearts shared features with established features of human cardiac aging, including increased hypertrophy and fibrosis as well as reduced fractional shortening, increased left atrial dimensions and decreased diastolic function[3]. Aged rat CM also shared features of remodeling with CM from rat hearts subjected to pressure overload. While heart weight showed a similar increase in aging to that in mild stenosis, the decreased function and increased fibrosis detected in aging was only present in response to severe stenosis, albeit at a greater extent than in aging. As in human, rat CM transitioned from a basal to a more pathology-related state in aging and pathology. Similarly, CM heterogeneity increased with age and in response to AB, which was again most increased in response to severe stenosis.

Although the number of DEGs identified in rats was relatively limited, potentially owing to the lower number of nuclei and samples analyzed than in human, the correlation of these genes with those identified in human aging and pathology supports their translational relevance and the value of the rat models to study pathology and aging. Importantly, we identified multiple genes representing functions similarly altered by aging and disease across species. Upregulated genes involved in cellular stress responses (*MKNK2* [124]), ECM remodeling (*CSGALNACT2* [125]), lipid metabolism (*DGKI* [126]), apoptosis regulation (*XKR4* [127]), inflammatory responses (IL6R [128]), and TGF-β signaling inhibition (*SMAD7* [108]). In pathology, human and rat CM showed elevated expression of *NPPA* (a cardiomyocyte stress marker [129]), *PLCE1* (which promotes IL-6-mediated inflammation [130], and *TGFB2* (a driver of fibrosis [129]). These shared molecular changes between rat and human reflect the role of inflammatory and fibrotic remodeling in CMPs from both species. Exemplifying a common pattern of response of rat and human with increased severity of hemodynamic stress, the greatest alteration in expression of genes encoding ion channels, calcium handling machinery components and respiration was detected in tight stenosis and ICM, which was lower in the other human CMP and mild stenosis in rat, and further reduced in aging in both species. Changes relevant to HF included decreased expression of potassium channels involved in cell repolarization, increased expression of calcium channels underlying action potential duration and decreased expression of genes involved in calcium handling. Together, these changes could underlie decreased contractile strength, slower relaxation and increased arrhythmia propensity of the diseased heart. This relationship between rat and human was also detected in a correlation analysis across all genes, particularly between severe stenosis in rat and ICM in human, highlighting convergence of pathways in end-stage HF.

In contrast to human, where no shared TFs were identified between aging and pathology, *Taf1* was

identified as a TF motif shared among the upregulated DEGs in both aging and pathological conditions in rats. Notably, the bromodomain-containing protein TAF1, which recognizes acetylated histones to regulate cardiac transcription programs, has been implicated in an epigenetically-driven mechanism of congenital heart disease (CHD), where disabling variants prevent its interaction with acetylated chromatin and disrupt normal gene expression [131]. These findings highlight the intricate regulatory landscape involving diverse transcription factors in the context of aging and cardiac pathologies, with potential implications for understanding molecular mechanisms and therapeutic strategies.

**In pathology and aging, rat and human CM share variable genes.**

Comparing the variable genes identified in aging and pathology in humans and rats, we observed several notable patterns. FNIP2/*Fnip2* (involved in cellular metabolism and energy regulation [82]) exhibited greater variation in DCM and HCM and showed high variability in the mild stenosis group in rats. GPM6A/*Gpm6a* (associated with stress responses [83]) demonstrated higher variation in the mild stenosis group in rats and was also highly variable in HCM, DCM, and aging samples in humans. PPARGC1A/*Ppargc1a* (a master regulator of mitochondrial biogenesis and energy metabolism [80]) showed increased variation in aged and ICM samples in humans, while in rats, higher variability was noted in the mild stenosis group. Similarly, PIK3R1/*Pik3r1* (involved in cell growth, metabolism, and survival [85]) had greater variation in DCM and ICM in humans and in the mild stenosis group in rats. NUAK1/*Nuak1* (associated with energy metabolism, cell survival, and stress response [87]) exhibited high variability in ICM and HCM in humans and in severe stenosis in rats. Finally, PER3/*Per3* (involved in circadian rhythms [90]) showed higher variation in DCM and ICM in humans and in the severe stenosis group in rats. These findings suggest that genes involved in cellular metabolism, energy regulation, stress response, and circadian rhythms exhibit conserved patterns of variability across species in the context of cardiac aging and disease.

**Fibrosis differs between rats and human and involves CM ECM-related gene expression**

Greater fibrosis/collagen deposition detected by histological staining is a recognized feature of the aged and diseased heart in both human [22, 132], and, as we describe here, in rat during aging and severe stenosis. Despite this histological evidence, an increase in mRNA abundance of pro-fibrotic genes was not consistently detected in our RT-qPCR analysis of RNA isolated from aged and diseased rat and human tissue. In particular, in rat, HF induced by severe stenosis and aging were both associated with increased tissue-level expression of fibrotic markers such as collagen 3 (*Col3a1*) and periostin (*Postn*), although in aging, gene expression changes were restricted to periostin. Fibrosis was less apparent in rats with mild stenosis, where gene expression changes were limited to upregulation of *Col3a1*. This data in rats contrasts with our analysis in human where an increase in tissue-level fibrotic gene expression was restricted to ICM and DCM. Notably and consistent with these mRNA analyses, we detected an increased proportion of FB in ICM and DCM but not in aging and HCM. Pro-fibrotic gene expression, FB proportion and fibrosis may not always, however, align. Indeed, no change in FB proportion despite increased ECM was previously reported in human aging [18]. However, the expression of pro-fibrotic genes and the proportion of FB that belonged to activated cell states involved in fibrotic remodeling are shown to be increased [18, 22]. These changes in FB cell states and gene expression provide a mechanism to maintain existing fibrosis without an increase in FB numbers. In human aging, and in contrast to rat, the interstitial fibrosis develops over decades, thereby reducing the requirement for the substantial augmentation of pro-fibrotic gene expression observed in pathology, where in response to damage or pathological cues, FB are rapidly engaged (increased proliferation, activation and gene expression) to maintain cardiac integrity and function [133]. The absence of an increased FB proportion in age and CMP could also be explained by biases in the extraction of cells prior to snRNA-Seq. However, the use of cardiac cell nuclei from frozen tissue has been shown by several laboratories to avoid this potential problem [134, 135]. The similarity of snRNA-Seq data to those obtained by RT-qPCR analysis of RNA isolated from tissue, further exclude reduced recovery of the nuclei of different cell types from fibrotic tissue as a confounder. Given the relatively small volume of the tissue processed for sequencing, differences in fibrosis across the heart may also contribute differences in discrepancies between histologically determined fibrosis and FB proportion, pro-fibrotic gene expression and FB states. FB numbers per tissue volume could also be increased or decreased without affecting their proportion relative to the total number of cells in the tissue if accompanied by changes in numbers or size of other cell types and/or changes in ECM mass. As well as the above discussed role of FB in fibrotic remodelling, we described in the snRNA-Seq analysis a consistent high expression of genes contributing to the ECM by CM during aging. Although this CM ECM-related signal was not detected in the analysis of bulk tissue mRNA, the identification of CM-

associated ECM gene expression [9] in the single nucleus sequencing data suggests that CM can also contribute to matrix remodeling and that they should be considered alongside FB when developing strategies to ameliorate fibrosis.

## Conclusion

Our integrative meta-analysis of snRNA-Seq data of CM across age and CMP in human and rat CM provides new insights into the shared and unique features of these forms of cardiac remodelling. Our study highlights shared features of age and pathology but also identifies differences that distinguish these forms of cardiac remodeling as distinct entities. In general, gene expression and gene expression trajectories indicate that pathology is not just a more severe form of aging. However, for certain gene categories, HF drives enrichment for gene expression changes that underlie the functional alterations associated with pathology. Notably, by comparing ICM in Y versus O human, we show an exacerbation of disease by age. Increased cellular heterogeneity is a clear shared feature across species and aging that can have key functional consequences. Our data suggest a contribution of deregulation of transcriptional control mechanisms to the development of cellular and transcriptional heterogeneity. Although our analysis was primarily bioinformatic, replication of some findings in an independent cardiac tissue collection, the presence of established markers of CM remodelling within our integrated analysis, and literature support for roles in CM remodelling for candidate targets identified in our datasets together validate our approach. However, additional functional analysis is required for validation of novel targets. These data suggest that future therapeutic interventions should look beyond late-stage symptom management. Potential strategies include targeting epigenetic regulators to mitigate against adverse transcriptional remodelling, cell state changes and the increases in cellular heterogeneity associated with aging in NF CM hearts.

## Limitations and future directions

While the study provides a comprehensive analysis of transcriptional alterations in CM, our study has some limitations. Although the human sn transcriptomics data integrated analysis was supported by leave-one-study-out sensitivity testing, residual confounders from study-specific technical factors and sample type imbalance across studies cannot be fully excluded. Sequencing chemistry and platform, nuclear isolation strategy, read depth, and preprocessing pipeline were partly confounded with source dataset. In addition, some disease groups were not uniformly represented across all datasets, limiting the extent to which individual comparisons could be tested independently of study origin. Therefore, we interpret the strongest findings at the level of recurrent transcriptional programs and pathway-level signatures, whereas individual genes are presented as candidate markers or regulatory features requiring validation. A further consideration is that while our "non-failing" hearts are designated as such due to absence of diagnosed pathology in medical records or at harvest, occult pathology cannot be excluded, particularly during aging. As such, DEGs specific to aging ICM vs NF aging, should be interpreted as transcriptional features enriched in NF aging rather than as definitive markers of healthy vs pathological aging. Similarly, while genes enriched in older NF hearts suggest protective or resilience-associated properties, future functional analysis is required to validate these findings. However, it is important to note that we study a normal human population making these detected changes relevant to this population. Additionally, the study primarily focuses on transcriptomic changes, and integrating other omics data, including proteomics and epigenomics [136], would provide further insight. While both sexes were included in the human study, albeit biased towards male according to the established prevalence of disease, the studies in rodents were performed only in male.

## Acknowledgments

We thank members of the Laboratory of Experimental Cardiology, KU Leuven for support, discussions and contributions to tissue biobanking and sample analysis. Roxane Menten is thanked for technical assistance and coordination of biobanking. We thank the UZ Leuven Transplant Team, the transplant coordinators, and Members of the UZ Leuven Cardiac Surgery Department for tissue procurement. This work was supported by project grants G0C6419N to HLR, G0C7319N and G026826N to KRS and FR, and G097021N to KS and HLR from the Flemish Research Council (FWO; Fonds Wetenschappelijk Onderzoek), by C1 grants C14/17/088 (HLR) and C14/21/093 (HLR, KS, FR) from the research fund of KU Leuven and the KG Jebsen Cardiac Research Center (IS and HLR). SE-T received a research grant from the Belgian Heart Fund, the Fund Walckiers-Van Dessel and the Fund Fernand Léonard in Basic Research in Cardiology managed by the King Baudouin Foundation (2024-J1190990-0019030). ELR thanks KU Leuven for support. OR thanks KU Leuven (PDMT1/21/030) and the FWO (12D6523N for Postdoctoral fellowship support. The authors acknowledge the KU Leuven Flow and Mass Cytometry core facility for cell sorting support and The Oslo Preclinical MR Core Facility, represented by Lili

Zhang and Vidar Skulberg for technical assistance. We acknowledge Prof Vincent Pasque for providing us with initial access to the VSC HPC project credits and San Kit To for the instructions for the initial computation at the server. The HPC resources and services used in this work were provided by the VSC (Flemish Supercomputer Center), funded by the Research Foundation - Flanders (FWO) and the Flemish Government.

## Conflict of Interest

All other authors declare no conflicts of interest.

## Author contributions

Conceptualisation: H.L.R., K.R.S. Data Curation: M.Y., K.R.S., S.E-T., H.L.R. Formal Analysis: S.E-T., H.L.R, E.C. R.D.P, M.Y., E.E., M.A., I.S. Funding acquisition: H.L.R., K.R.S., S.E-T., O.R., I.S. Investigation: S.E-T., H.L.R, E.C. E.L.R., R.D.P., M.S., M.A., E.S., I.S., E.E, L.L. Methodology: H.L.R., K.R.S, S.E-T., R.D.P., B.T., E.E, E.L.R., O.R., Supervision: H.L.R., K.R.S., I.S. Visualization: S.E-T, R.D.P, H.L.R. Writing – original Draft: S.E-T., R.D.P, H.L.R. Writing – review and editing: All. Resources: K.C.B, K.B.M., K.A., O.B., F.R., I.S., E.E., M.Y., H.L.R. and K.R.S.

## Supplementary Materials

The Supplementary data comprising Supplementary Figures, Tables, Extended methods and Supplementary data files can be found online at www.aginganddisease.org/EN/10.14336/AD.2026.0357.

## References

[1] Roth GA, Mensah GA, Johnson CO, Addolorato G, Ammirati E, Baddour LM, et al. (2020). Global Burden of Cardiovascular Diseases and Risk Factors, 1990-2019: Update From the GBD 2019 Study. J Am Coll Cardiol, 76:2982–3021.

[2] Timmis A, Aboyans V, Vardas P, Townsend N, Torbica A, Kavousi M, et al. (2024). European Society of Cardiology: the 2023 Atlas of Cardiovascular Disease Statistics. Eur Heart J, 45:4019–4062.

[3] Abdellatif M, Rainer PP, Sedej S, Kroemer G (2023). Hallmarks of cardiovascular aging. Nat Rev Cardiol, 20:754–777.

[4] Hastings MH, Zhou Q, Wu C, Shabani P, Huang S, Yu X, et al. (2025). Cardiac aging: from hallmarks to therapeutic opportunities. Cardiovasc Res, 121:1474–1488.

[5] Tracy E, Rowe G, LeBlanc AJ (2020). Cardiac tissue remodeling in healthy aging: the road to pathology. Am J Physiol Cell Physiol, 319:C166–C182.

[6] Guo J, Huang X, Dou L, Yan M, Shen T, Tang W, et al. (2022). Aging and aging-related diseases: from molecular mechanisms to interventions and treatments. Signal Transduct Target Ther, 7:391.

[7] Schaum N, Lehallier B, Hahn O, Palovics R, Hosseinzadeh S, Lee SE, et al. (2020). Aging hallmarks exhibit organ-specific temporal signatures. Nature, 583:596–602.

[8] Vakka A, Warren JS, Drosatos K (2023). Cardiovascular aging: from cellular and molecular changes to therapeutic interventions. J Cardiovasc Aging, 3:23

[9] Vidal R, Wagner JUG, Braeuning C, Fischer C, Patrick R, Tombor L, et al. (2019). Transcriptional heterogeneity of fibroblasts is a hallmark of the aging heart. JCI Insight, 4:a035428.

[10] Preissl S, Schwaderer M, Raulf A, Hesse M, Gruning BA, Kobele C, et al. (2015). Deciphering the Epigenetic Code of Cardiac Myocyte Transcription. Circ Res, 117:413–423.

[11] Thienpont B, Aronsen JM, Robinson EL, Okkenhaug H, Loche E, Ferrini A, et al. (2017). The H3K9 dimethyltransferases EHMT1/2 protect against pathological cardiac hypertrophy. J Clin Invest, 127:335–348.

[12] Bahar R, Hartmann CH, Rodriguez KA, Denny AD, Busuttil RA, Dolle ME, et al. (2006). Increased cell-to-cell variation in gene expression in aging mouse heart. Nature, 441:1011–1014.

[13] Gilbert G, Demydenko K, Dries E, Puertas RD, Jin X, Sipido K, et al. (2020). Calcium Signaling in Cardiomyocyte Function. Cold Spring Harbor Perspectives in Biology, 12:a035428.

[14] de Lucia C, Eguchi A, Koch WJ (2018). New Insights in Cardiac beta-Adrenergic Signaling During Heart Failure and Aging. Front Pharmacol, 9:904.

[15] Takahashi T, Schunkert H, Isoyama S, Wei JY, Nadal-Ginard B, Grossman W, et al. (1992). Age-related differences in the expression of proto-oncogene and contractile protein genes in response to pressure overload in the rat myocardium. J Clin Invest, 89:939–946.

[16] Nomura S, Satoh M, Fujita T, Higo T, Sumida T, Ko T, et al. (2018). Cardiomyocyte gene programs encoding morphological and functional signatures in cardiac hypertrophy and failure. Nat Commun, 9:4435.

[17] Chaffin M, Papangeli I, Simonson B, Akkad AD, Hill MC, Arduini A, et al. (2022). Single-nucleus profiling of human dilated and hypertrophic cardiomyopathy. Nature, 608:174–180.

[18] Koenig AL, Shchukina I, Amrute J, Andhey PS, Zaitsev K, Lai L, et al. (2022). Single-cell transcriptomics reveals cell-type-specific diversification in human heart failure. Nat Cardiovasc Res, 1:263–280.

[19] Kuppe C, Ramirez Flores RO, Li Z, Hayat S, Levinson RT, Liao X, et al. (2022). Spatial multi-omic map of human myocardial infarction. Nature, 608:766–777.

[20] Litvinukova M, Talavera-Lopez C, Maatz H, Reichart D, Worth CL, Lindberg EL, et al. (2020). Cells of the adult human heart. Nature, 588:466–472.

[21] Amoni M, Vermoortele D, Ekhteraei-Tousi S, Donate Puertas R, Gilbert G, Youness M, et al. (2023).

Heterogeneity of Repolarization and Cell-Cell Variability of Cardiomyocyte Remodeling Within the Myocardial Infarction Border Zone Contribute to Arrhythmia Susceptibility. Circ Arrhythm Electrophysiol, 16:e011677.

[22] Youness M, Ekhteraei-Tousi S, Nagaraju CK, Puertas RD, Thienpont B, Rega F, et al. (2025). Location and aetiology are determinants of fibroblast activation and heterogeneity in the failing human heart. Genome Med, 17:155.

[23] Chen CY, Caporizzo MA, Bedi K, Vite A, Bogush AI, Robison P, et al. (2018). Suppression of detyrosinated microtubules improves cardiomyocyte function in human heart failure. Nat Med, 24:1225–1233.

[24] Robison P, Caporizzo MA, Ahmadzadeh H, Bogush AI, Chen CY, Margulies KB, et al. (2016). Detyrosinated microtubules buckle and bear load in contracting cardiomyocytes. Science, 352:aaf0659.

[25] Hauge-Iversen IM, Norden ES, Melleby AO, Espeland L, Zhang L, Sjaastad I, et al. (2025). Non-invasive estimation of left ventricular chamber stiffness using cardiovascular magnetic resonance and echocardiography. J Cardiovasc Magn Reson, 27:101849.

[26] Bankhead P, Loughrey MB, Fernandez JA, Dombrowski Y, McArt DG, Dunne PD, et al. (2017). QuPath: Open source software for digital pathology image analysis. Sci Rep, 7:16878.

[27] Muraro MJ, Dharmadhikari G, Grun D, Groen N, Dielen T, Jansen E, et al. (2016). A Single-Cell Transcriptome Atlas of the Human Pancreas. Cell Syst, 3:385–394 e383.

[28] Hashimshony T, Wagner F, Sher N, Yanai I (2012). CEL-Seq: Single-Cell RNA-Seq by Multiplexed Linear Amplification. Cell Reports, 2:666–673.

[29] Vandesompele J, De Preter K, Pattyn F, Poppe B, Van Roy N, De Paepe A, et al. (2002). Accurate normalization of real-time quantitative RT-PCR data by geometric averaging of multiple internal control genes. Genome Biol, 3:RESEARCH0034.

[30] Salmen F, De Jonghe J, Kaminski TS, Alemany A, Parada GE, Verity-Legg J, et al. (2022). High-throughput total RNA sequencing in single cells using VASA-seq. Nat Biotechnol, 40:1780–1793.

[31] Fu Y, Youness M, Virzi A, Song X, Tubeeckx MRL, De Keulenaer GW, et al. (2025). Benchmarking of computational demultiplexing methods for single-nucleus RNA sequencing data. Brief Bioinform, 26:bbaf371.

[32] Street K, Risso D, Fletcher RB, Das D, Ngai J, Yosef N, et al. (2018). Slingshot: cell lineage and pseudotime inference for single-cell transcriptomics. Bmc Genomics, 19:477.

[33] Lun ATL, Marioni JC (2017). Overcoming confounding plate effects in differential expression analyses of single-cell RNA-seq data. Biostatistics, 18:451–464.

[34] Squair JW, Gautier M, Kathe C, Anderson MA, James ND, Hutson TH, et al. (2021). Confronting false discoveries in single-cell differential expression. Nat Commun, 12:5692.

[35] Alboukadel Kassambara FM. 2020. factoextra: Extract and Visualize the Results of Multivariate Data Analyses.: R package.

[36] Leek JT JW, Parker HS, Fertig EJ, Jaffe AE, Zhang Y, Storey JD, Torres LC. 2023. sva: Surrogate Variable Analysis.: R package.

[37] Robinson MD, McCarthy DJ, Smyth GK (2010). edgeR: a Bioconductor package for differential expression analysis of digital gene expression data. Bioinformatics, 26:139–140.

[38] McCarthy DJ, Chen Y, Smyth GK (2012). Differential expression analysis of multifactor RNA-Seq experiments with respect to biological variation. Nucleic Acids Res, 40:4288–4297.

[39] Chen Y, Lun AT, Smyth GK (2016). From reads to genes to pathways: differential expression analysis of RNA-Seq experiments using Rsubread and the edgeR quasi-likelihood pipeline. F1000Res, 5:1438.

[40] Wu T, Hu E, Xu S, Chen M, Guo P, Dai Z, et al. (2021). clusterProfiler 4.0: A universal enrichment tool for interpreting omics data. Innovation (Camb), 2:100141.

[41] Yu G, Wang LG, Han Y, He QY (2012). clusterProfiler: an R package for comparing biological themes among gene clusters. OMICS, 16:284–287.

[42] Kuleshov MV, Jones MR, Rouillard AD, Fernandez NF, Duan Q, Wang Z, et al. (2016). Enrichr: a comprehensive gene set enrichment analysis web server 2016 update. Nucleic Acids Res, 44:W90–97.

[43] Aibar Sara ea. 2016. RcisTarget: Identify transcription factor binding motifs enriched on a gene list. R/Bioconductor package.

[44] Aibar S, Gonzalez-Blas CB, Moerman T, Huynh-Thu VA, Imrichova H, Hulselmans G, et al. (2017). SCENIC: single-cell regulatory network inference and clustering. Nat Methods, 14:1083–1086.

[45] Dusa A. 2021. venn: Draw Venn Diagrams.: CRAN.

[46] Walter W, Sanchez-Cabo F, Ricote M (2015). GOplot: an R package for visually combining expression data with functional analysis. Bioinformatics, 31:2912–2914.

[47] Lex A, Gehlenborg N, Strobelt H, Vuillemot R, Pfister H (2014). UpSet: Visualization of Intersecting Sets. IEEE Trans Vis Comput Graph, 20:1983–1992.

[48] Brian G. Peterson PC. 2020. PerformanceAnalytics: Econometric Tools for performance and Risk Analysis. CRAN.

[49] Langfelder P, Horvath S (2008). WGCNA: an R package for weighted correlation network analysis. BMC Bioinformatics, 9:559.

[50] Gabor Csardi TN. 2006. The igraph software package for complex network research. In InterJournal.

[51] Pedersen TL. 2021. ggraph: An Implementation of Grammar of Graphics for Graphs and Networks.

[52] Durinck S, Moreau Y, Kasprzyk A, Davis S, De Moor B, Brazma A, et al. (2005). BioMart and Bioconductor: a powerful link between biological databases and microarray data analysis. Bioinformatics, 21:3439–3440.

[53] Wickham H AM, Bryan J, Chang W, McGowan LD, François R, Grolemund, G HA, Henry L, Hester J, Kuhn M, Pedersen TL, Miller E, Bache SM, Müller K OJ,

Robinson D, Seidel DP, Spinu V, Takahashi K, Vaughan D, Wilke C WK, Yutani H (2019). Welcome to the Tidyverse. The Journal of Open Source Software, 4.
[54] Hadley Wickham RF, Lionel Henry and Kirill Müller. 2021. dplyr: A Grammar of Data Manipulation.: CRAN.
[55] Wickham H. 2016. ggplot2: Elegant Graphics for Data Analysis.: Springer-Verlag New York.
[56] Kassambara A. 2020. ggpubr: 'ggplot2' Based Publication Ready Plots.: CRAN.
[57] Bunis DG, Andrews J, Fragiadakis GK, Burt TD, Sirota M (2021). dittoSeq: universal user-friendly single-cell and bulk RNA sequencing visualization toolkit. Bioinformatics, 36:5535–5536.
[58] Miyata N, Watanabe Y, Tamura Y, Endo T, Kuge O (2016). Phosphatidylserine transport by Ups2-Mdm35 in respiration-active mitochondria. J Cell Biol, 214:77–88.
[59] Putku M, Kals M, Inno R, Kasela S, Org E, Kozich V, et al. (2015). CDH13 promoter SNPs with pleiotropic effect on cardiometabolic parameters represent methylation QTLs. Hum Genet, 134:291–303.
[60] Anfinson M, Fitts RH, Lough JW, James JM, Simpson PM, Handler SS, et al. (2022). Significance of alpha-Myosin Heavy Chain (MYH6) Variants in Hypoplastic Left Heart Syndrome and Related Cardiovascular Diseases. J Cardiovasc Dev Dis, 9:144.
[61] Mikhailov AT, Torrado M (2008). The enigmatic role of the ankyrin repeat domain 1 gene in heart development and disease. Int J Dev Biol, 52:811–821.
[62] Kwapiszewska G, Wygrecka M, Marsh LM, Schmitt S, Trosser R, Wilhelm J, et al. (2008). Fhl-1, a new key protein in pulmonary hypertension. Circulation, 118:1183–1194.
[63] Fittipaldi S, Mercatelli N, Dimauro I, Jackson MJ, Paronetto MP, Caporossi D (2015). Alpha B-crystallin induction in skeletal muscle cells under redox imbalance is mediated by a JNK-dependent regulatory mechanism. Free Radic Biol Med, 86:331–342.
[64] Rajakumari S, Wu J, Ishibashi J, Lim HW, Giang AH, Won KJ, et al. (2013). EBF2 determines and maintains brown adipocyte identity. Cell Metab, 17:562–574.
[65] Zhang Y, Xu D, Huang H, Chen S, Wang L, Zhu L, et al. (2014). Regulation of glucose homeostasis and lipid metabolism by PPP1R3G-mediated hepatic glycogenesis. Mol Endocrinol, 28:116–126.
[66] de Ruijter AJ, van Gennip AH, Caron HN, Kemp S, van Kuilenburg AB (2003). Histone deacetylases (HDACs): characterization of the classical HDAC family. Biochem J, 370:737–749.
[67] Pohjolainen L, Kinnunen SM, Auno S, Kiriazis A, Pohjavaara S, Kari-Koskinen J, et al. (2024). Switching of hypertrophic signaling towards enhanced cardiomyocyte identity and maturity by a GATA4-targeted compound. Stem Cell Res Ther, 15:5.
[68] Dong C, Nakagawa R, Oyama K, Yamamoto Y, Zhang W, Dong A, et al. (2020). Structural basis for histone variant H3tK27me3 recognition by PHF1 and PHF19. Elife, 9:e58675.
[69] Shi Z, Xu S, Xing S, Yao K, Zhang L, Xue L, et al. (2019). Mettl17, a regulator of mitochondrial ribosomal RNA modifications, is required for the translation of mitochondrial coding genes. FASEB J, 33:13040–13050.
[70] Salameh A, Lee AK, Cardo-Vila M, Nunes DN, Efstathiou E, Staquicini FI, et al. (2015). PRUNE2 is a human prostate cancer suppressor regulated by the intronic long noncoding RNA PCA3. Proc Natl Acad Sci U S A, 112:8403–8408.
[71] Lopez-Otin C, Blasco MA, Partridge L, Serrano M, Kroemer G (2023). Hallmarks of aging: An expanding universe. Cell, 186:243–278.
[72] de la Pena Avalos B, Tropee R, Duijf PHG, Dray E (2023). EYA4 promotes breast cancer progression and metastasis through its role in replication stress avoidance. Mol Cancer, 22:158.
[73] Foy RL, Song IY, Chitalia VC, Cohen HT, Saksouk N, Cayrou C, et al. (2008). Role of Jade-1 in the histone acetyltransferase (HAT) HBO1 complex. J Biol Chem, 283:28817–28826.
[74] Fan Z, Yamaza T, Lee JS, Yu J, Wang S, Fan G, et al. (2009). BCOR regulates mesenchymal stem cell function by epigenetic mechanisms. Nat Cell Biol, 11:1002–1009.
[75] He Y, Wang S, Liu S, Qin D, Liu Z, Wang L, et al. (2023). MSL1 Promotes Liver Regeneration by Driving Phase Separation of STAT3 and Histone H4 and Enhancing Their Acetylation. Adv Sci (Weinh), 10:e2301094.
[76] Abdouh M, Hanna R, El Hajjar J, Flamier A, Bernier G (2016). The Polycomb Repressive Complex 1 Protein BMI1 Is Required for Constitutive Heterochromatin Formation and Silencing in Mammalian Somatic Cells. J Biol Chem, 291:182–197.
[77] Le Thomas A, Rogers AK, Webster A, Marinov GK, Liao SE, Perkins EM, et al. (2013). Piwi induces piRNA-guided transcriptional silencing and establishment of a repressive chromatin state. Genes Dev, 27:390–399.
[78] Noguchi K, Iwasaki K, Ishikawa I (1999). Prostaglandin F2 alpha upregulates intercellular adhesion molecule-1 expression in human gingival fibroblasts. J Periodontal Res, 34:277–281.
[79] Xu JX, Tang ML, Lu ZF, Song Y, Zhang KL, He RC, et al. (2023). A novel role for YPEL2 in mediating endothelial cellular senescence via the p53/p21 pathway. Mech Aging Dev, 211:111803.
[80] Fernandez-Marcos PJ, Auwerx J (2011). Regulation of PGC-1alpha, a nodal regulator of mitochondrial biogenesis. Am J Clin Nutr, 93:884S–890.
[81] M NK, V BSCT, G KV, B CS, Guntupalli S, J SB (2016). Molecular characterization of human ABHD2 as TAG lipase and ester hydrolase. Biosci Rep, 36.
[82] Fernandez LP, Deleyto-Seldas N, Colmenarejo G, Sanz A, Wagner S, Plata-Gomez AB, et al. (2022). Folliculin-interacting protein FNIP2 impacts on overweight and obesity through a polymorphism in a conserved 3' untranslated region. Genome Biol, 23:230.
[83] Sayed A, Turoczi S, Soares-da-Silva F, Marazzi G, Hulot JS, Sassoon D, et al. (2022). Hypoxia promotes a perinatal-like progenitor state in the adult murine epicardium. Sci Rep, 12:9250.
[84] Wolfe AL, Zhou Q, Toska E, Galeas J, Ku AA, Koche RP, et al. (2021). UDP-glucose pyrophosphorylase 2, a

regulator of glycogen synthesis and glycosylation, is critical for pancreatic cancer growth. Proc Natl Acad Sci U S A, 118.

[85] Gupta I, Gaykalova DA (2024). Unveiling the role of PIK3R1 in cancer: A comprehensive review of regulatory signaling and therapeutic implications. Semin Cancer Biol, 106-107:58–86.

[86] Bucardo MS, Wu Y, Ludford PT, 3rd, Li Y, Fin A, Tor Y (2021). Real-Time Monitoring of Human Guanine Deaminase Activity by an Emissive Guanine Analog. ACS Chem Biol, 16:1208–1214.

[87] Port J, Muthalagu N, Raja M, Ceteci F, Monteverde T, Kruspig B, et al. (2018). Colorectal Tumors Require NUAK1 for Protection from Oxidative Stress. Cancer Discov, 8:632–647.

[88] Wu X, Ivanchenko MV, Al Jandal H, Cicconet M, Indzhykulian AA, Corey DP (2019). PKHD1L1 is a coat protein of hair-cell stereocilia and is required for normal hearing. Nat Commun, 10:3801.

[89] Morange PE, Saut N, Alessi MC, Yudkin JS, Margaglione M, Di Minno G, et al. (2007). Association of plasminogen activator inhibitor (PAI)-1 (SERPINE1) SNPs with myocardial infarction, plasma PAI-1, and metabolic parameters: the HIFMECH study. Arterioscler Thromb Vasc Biol, 27:2250–2257.

[90] Noda M, Iwamoto I, Tabata H, Yamagata T, Ito H, Nagata KI (2019). Role of Per3, a circadian clock gene, in embryonic development of mouse cerebral cortex. Sci Rep, 9:5874.

[91] Zhu Y, Zou R, Sha H, Lu Y, Zhang Y, Wu J, et al. (2020). Lipid metabolism-related proteins of relevant evolutionary and lymphoid interest (PRELI) domain containing family proteins in cancer. Am J Transl Res, 12:6015–6026.

[92] Huang L, Wu KH, Zhang L, Wang Q, Tang S, Wu Q, et al. (2018). Critical Roles of Xirp Proteins in Cardiac Conduction and Their Rare Variants Identified in Sudden Unexplained Nocturnal Death Syndrome and Brugada Syndrome in Chinese Han Population. J Am Heart Assoc, 7:e006320.

[93] Wu Y, Chen S, Huang G, Zhang L, Zhong L, Feng Y, et al. (2024). Transcriptome analysis reveals EBF1 ablation-induced injuries in cardiac system. Theranostics, 14:4894–4915.

[94] Kim EE, Shekhar A, Ramachandran J, Khodadadi-Jamayran A, Liu FY, Zhang J, et al. (2023). The transcription factor EBF1 non-cell-autonomously regulates cardiac growth and differentiation. Development, 150:dev202054.

[95] Song Y, Spurlock B, Liu J, Qian L (2024). Cardiac Aging in the Multi-Omics Era: High-Throughput Sequencing Insights. Cells, 13:1683.

[96] Barrick SK, Greenberg MJ (2021). Cardiac myosin contraction and mechanotransduction in health and disease. Journal of Biological Chemistry, 297:101297.

[97] Man J, Barnett P, Christoffels VM (2018). Structure and function of the Nppa-Nppb cluster locus during heart development and disease. Cell Mol Life Sci, 75:1435–1444.

[98] Stefano Strocchi CS-F, David Bode, Simone Jung, Gabriele Schiattarella, (2022). Aging-specific changes in cardiomyocyte transcriptome at single-cell resolution,. Journal of Molecular and Cellular Cardiology,, 173:S51–S52.

[99] Barefield D, Kumar M, de Tombe PP, Sadayappan S (2014). Contractile dysfunction in a mouse model expressing a heterozygous MYBPC3 mutation associated with hypertrophic cardiomyopathy. Am J Physiol Heart Circ Physiol, 306:H807–815.

[100] de Frutos F, Ochoa JP, Navarro-Penalver M, Baas A, Bjerre JV, Zorio E, et al. (2022). Natural History of MYH7-Related Dilated Cardiomyopathy. J Am Coll Cardiol, 80:1447–1461.

[101] Fukuda R, Gunawan F, Ramadass R, Beisaw A, Konzer A, Mullapudi ST, et al. (2019). Mechanical Forces Regulate Cardiomyocyte Myofilament Maturation via the VCL-SSH1-CFL Axis. Dev Cell, 51:62–77 e65.

[102] Assendorp N, Fossati M, Libe-Philippot B, Christopoulou E, Depp M, Rapone R, et al. (2024). CTNND2 moderates the pace of synaptic maturation and links human evolution to synaptic neoteny. Cell Rep, 43:114797.

[103] Derumeaux G, Sawaki D, Czibik G (2024). Trajectories in Cardiac Aging: Journey to the Crossroads of Inflammation and Metabolism. Circulation, 149:1935–1937.

[104] Brundage J, Barrios JP, Tison GH, Pirruccello JP (2024). Genetics of Cardiac Aging Implicate Organ-Specific Variation. medRxiv 2024.08.02.243108.

[105] Kuwayama N, Kujirai T, Kishi Y, Hirano R, Echigoya K, Fang L, et al. (2023). HMGA2 directly mediates chromatin condensation in association with neuronal fate regulation. Nat Commun, 14:6420.

[106] Lau L, Porciuncula A, Yu A, Iwakura Y, David G (2019). Uncoupling the Senescence-Associated Secretory Phenotype from Cell Cycle Exit via Interleukin-1 Inactivation Unveils Its Protumorigenic Role. Mol Cell Biol, 39:e00586-18.

[107] Riddell A, McBride M, Braun T, Nicklin SA, Cameron E, Loughrey CM, et al. (2020). RUNX1: an emerging therapeutic target for cardiovascular disease. Cardiovascular Research, 116:1410–1423.

[108] Chen Q, Chen H, Zheng D, Kuang C, Fang H, Zou B, et al. (2009). Smad7 is required for the development and function of the heart. J Biol Chem, 284:292–300.

[109] Zhang L, Liu R, Luan YY, Yao YM (2018). Tumor Necrosis Factor-alpha Induced Protein 8: Pathophysiology, Clinical Significance, and Regulatory Mechanism. Int J Biol Sci, 14:398–405.

[110] Yang M, Ge J, Liu YL, Wang HY, Wang ZH, Li DP, et al. (2024). Sortilin-mediated translocation of mitochondrial ACSL1 impairs adipocyte thermogenesis and energy expenditure in male mice. Nat Commun, 15:7746.

[111] Schlaepfer IR, Joshi M (2020). CPT1A-mediated Fat Oxidation, Mechanisms, and Therapeutic Potential. Endocrinology, 161:bqz046.

[112] Byron A, Humphries JD, Humphries MJ (2013). Defining the extracellular matrix using proteomics. Int J Exp Pathol, 94:75–92.
[113] Simonson B, Chaffin M, Hill MC, Atwa O, Guedira Y, Bhasin H, et al. (2023). Single-nucleus RNA sequencing in ischemic cardiomyopathy reveals common transcriptional profile underlying end-stage heart failure. Cell Rep, 42:112086.
[114] Yuqi Tan AS, Michael Farid, Da Peng, Patrick Cahan. (2021). Quantitative comparison of in vitro and in vivo embryogenesis at a single cell resolution. bioRxiv:2021.05.07.443179.
[115] Li Y, Li Z, Zhang C, Li P, Wu Y, Wang C, et al. (2017). Cardiac Fibroblast-Specific Activating Transcription Factor 3 Protects Against Heart Failure by Suppressing MAP2K3-p38 Signaling. Circulation, 135:2041–2057.
[116] Cendula R, Chomanicova N, Adamickova A, Gazova A, Kyselovic J, Matus M (2021). Altered Expression of ORAI and STIM Isoforms in Activated Human Cardiac Fibroblasts. Physiol Res, 70:S21–S30.
[117] Panchenko MV (2016). Structure, function and regulation of jade family PHD finger 1 (JADE1). Gene, 589:1–11.
[118] Pereira MJ, Kamble PG, Jernow H, Kristófi R, Holbikova E, Skrtic S, et al. (2021). CDKN2C expression in adipose tissue is reduced in type II diabetes and central obesity: impact on adipocyte differentiation and lipid storage? Translational Research, 242:105-121.
[119] Choi J, Bachmann AL, Tauscher K, Benda C, Fierz B, Muller J (2017). DNA binding by PHF1 prolongs PRC2 residence time on chromatin and thereby promotes H3K27 methylation. Nat Struct Mol Biol, 24:1039–1047.
[120] Nasser J, Bergman DT, Fulco CP, Guckelberger P, Doughty BR, Patwardhan TA, et al. (2021). Genome-wide enhancer maps link risk variants to disease genes. Nature, 593:238–243.
[121] van der Harst P, Verweij N (2018). Identification of 64 Novel Genetic Loci Provides an Expanded View on the Genetic Architecture of Coronary Artery Disease. Circ Res, 122:433–443.
[122] Consortium GT (2020). The GTEx Consortium atlas of genetic regulatory effects across human tissues. Science, 369:1318–1330.
[123] Kim-Hellmuth S, Aguet F, Oliva M, Munoz-Aguirre M, Kasela S, Wucher V, et al. (2020). Cell type-specific genetic regulation of gene expression across human tissues. Science, 369:eaaz8528.
[124] Maimon A, Mogilevsky M, Shilo A, Golan-Gerstl R, Obiedat A, Ben-Hur V, et al. (2014). Mnk2 alternative splicing modulates the p38-MAPK pathway and impacts Ras-induced transformation. Cell Rep, 7:501–513.
[125] Sato T, Gotoh M, Kiyohara K, Akashima T, Iwasaki H, Kameyama A, et al. (2003). Differential roles of two N-acetylgalactosaminyltransferases, CSGalNAcT-1, and a novel enzyme, CSGalNAcT-2. Initiation and elongation in synthesis of chondroitin sulfate. J Biol Chem, 278:3063–3071.
[126] Liu W, Yuan W, Li X, Zhuang J, Mo X, Dai G, et al. (2018). ZNF424 Induces Apoptosis and Inhibits Proliferation in Lung Carcinoma Cells. Curr Mol Med, 18:109–115.
[127] Chakraborty S, Feng Z, Lee S, Alvarenga OE, Panda A, Zhang S, et al. (2025). Structure and function of the human apoptotic scramblase Xkr4. Nat Commun, 16:7317.
[128] Interleukin-6 Receptor Mendelian Randomisation Analysis C, Swerdlow DI, Holmes MV, Kuchenbaecker KB, Engmann JE, Shah T, et al. (2012). The interleukin-6 receptor as a target for prevention of coronary heart disease: a mendelian randomisation analysis. Lancet, 379:1214–1224.
[129] Martin-Garrido A, Heineke J (2025). Cardiomyocyte-derived fibrosis as driver of cardiomyopathy. Cardiovasc Res.121: 528-529.
[130] Li W, Li Y, Chu Y, Wu W, Yu Q, Zhu X, et al. (2019). PLCE1 promotes myocardial ischemia-reperfusion injury in H/R H9c2 cells and I/R rats by promoting inflammation. Biosci Rep, 39:BSR20181613.
[131] Leigh RS, Valimaki MJ, Kaynak BL, Ruskoaho HJ (2023). TAF1 bromodomain inhibition as a candidate epigenetic driver of congenital heart disease. Biochim Biophys Acta Mol Basis Dis, 1869:166689.
[132] Gazoti Debessa CR, Mesiano Maifrino LB, Rodrigues de Souza R (2001). Age related changes of the collagen network of the human heart. Mech Aging Dev, 122:1049–1058.
[133] Van Linthout S, Matz I, Gonzalez A, Davis J (2026). Cardiac fibroblasts in myocardial injury and heart failure. Eur Heart J, 47:2271–2285.
[134] Pimpalwar N, Czuba T, Smith ML, Nilsson J, Gidlof O, Smith JG (2020). Methods for isolation and transcriptional profiling of individual cells from the human heart. Heliyon, 6:e05810.
[135] Hu P, Liu J, Zhao J, Wilkins BJ, Lupino K, Wu H, et al. (2018). Single-nucleus transcriptomic survey of cell diversity and functional maturation in postnatal mammalian hearts. Genes Dev, 32:1344–1357.
[136] Malecki C, Guglielmi G, Hunter B, Harney D, Koay YC, Don AS, et al. (2025). The Human Cardiac "Age-OME": Age-Specific Changes in Myocardial Molecular Expression. Aging Cell, 24:e70219.